Thesis
and
Reports
Ranson
K. J.

EVALUATION OF ILLUMINATION AND TERRAIN GEOMETRY EFFECTS ON SPECTRAL RESPONSE IN MOUNTAIN TERRAIN

K. J. Ranson
J. Kramer
J. Kirchner
J. A. Smith

Final Report, Volume II

Rocky Mountain Forest and Range Experiment Station

U.S. Forest Service

Cooperative Agreement 16-741-CA

September, 1978

College of Forestry and Natural Resources

Colorado State University

Fort Collins, Colorado 80523

LIBRARY

FEB 16 1979

ROCKY MOUNTAIN STATI

EVALUATION OF ILLUMINATION AND TERRAIN GEOMETRY EFFECTS ON SPECTRAL RESPONSE IN MOUNTAIN TERRAIN

K. J. Ranson
J. Kramer
J. Kirchner
J. A. Smith

Final Report, Volume II

Rocky Mountain Forest and Range Experiment Station

U.S. Forest Service

Cooperative Agreement 16-741-CA

September, 1978

College of Forestry and Natural Resources

Colorado State University

Fort Collins, Colorado 80523

THE FINDINGS IN THIS REPORT ARE NOT TO BE CONSTRUED AS AN OFFICIAL U.S. FOREST SERVICE POSITION UNLESS SO DESIGNATED BY OTHER AUTHORIZED DOCUMENTS.

ABSTRACT

An extensive analysis of terrain geometric effects on the optical scattering properties of natural resource scene in mountainous terrain has been performed. Spectral reflectance measurements were obtained for lodgepole pine, *Pinus contorta*, ponderosa pine, *Pinus ponderosa*, Russian olive, *Eleaegnus angustifolia*, grass species, *Agropyron sp.*, and *Bromus sp.*, and snow. Sensor platforms included ground-based measurements using aerial tramways, aircraft radiometric observations, and satellite (Landsat) measurements. A wide range of effective view and source illumination angles were recorded for the various target/sensor combinations.

Regression analyses and photometric plots were made from the data in order to test the Lambertian assumption for the various material types. In addition a process-oriented radiative transfer model was applied to the data. This model was also used to evaluate initial effects of background topographic variations.

Results of this study indicate that, particularly in the chlorophyll absorption band all materials exhibit non-Lambertian behavior for effective zenith sensor or source angles greater than 60 degrees, but that for effective angles less than 40 degrees, the Lambertian assumption may be valid. For stable atmospheric conditions and constant phase angle the Minnaert relationship may be applied to quantify scene radiance properties. The canopy reflectance model was found to follow the general trends of the field measurements but overestimates infrared response. In order to adequately model topographic influences or spectral response, canopy density variations must be included.

FOREWORD

The research described in this report was supported by the U.S. Forest Service under Cooperative Agreement 16-741-CA, "Signature Studies for Natural Resource Inventory". It summarizes results obtained under Objective 2 of the project entitled, "Spectral Variability in Mountain Terrain". Mr. Robert Dana was technical monitor of this project. The purpose of this study was to evaluate the effects of such extrinsic variables as sun angle and terrain geometry on the spectral response of natural resource scenes. Field measurements, aerial and satellite observations, and canopy reflectance modeling were all utilized in this study.

Participating project personnel at various times included: Dr. James A. Smith, Principal Investigator; Mr. K. Jon Ranson, Research Associate; Mr. Steve Bernath, Research Associate; Mr. Jim Kramer, Graduate Research Assistant; Ms. Julie Kirchner, Graduate Research Assistant; Mr. Dan Kimes, Graduate Research Assistant; and Mr. Frank Itkowsky, Graduate Research Assistant.

Mr. Tzeu Lie Lin received the Master of Science degree for work related to project tasks as described in Chapter 2.3 of this report. It is anticipated that Chapter 2.2 will form the basis for a Master of Science paper for Mr. Jim Kramer.

The authors would like to express their appreciation to Mr. Robert Dana, particularly for his assistance in the execution and analysis of the aircraft radiance experiments, and to Dr. Richard Driscoll, Program Leader, Rocky Mountain Forest and Range Experiment Station, whose support made this work possible.

TABLE OF CONTENTS

Chapter		Page
	LIST OF FIGURES	i
	LIST OF TABLES	iii
1.0	INTRODUCTION	1
2.0	EXTRINSIC GEOMETRIC EFFECTS	3
	2.1 Data Acquisition for 1977-1978	5
	2.2 Aerial Tramway Sun Angle Experiments--Constrained View Angle and Topography Case	6
	2.2.1 Experimental Procedures	7
	2.2.2 Experimental Results	9
	2.2.3 Summary	17
	2.3 Analysis of Topographical Effects on Airborne Radiometer Data	19
	2.3.1 Instrumentation	19
	2.3.2 Study Site	20
	2.3.3 Data Reduction	21
	2.3.4 Analysis of Sample Points	25
	2.3.5 Summary	36
	2.4 The Lambertian Assumption and Landsat Data	36
	2.4.1 Analytical Background	37
	2.4.2 Data Reduction and Analysis	41
	2.4.3 Results	44
	2.4.4 Discussion and Recommendations	47
3.0	CANOPY MODELING	53
	3.1 Model Modifications	53
	3.2 Model Simulations	55
	3.2.1 Benchmark Comparisons	55
	3.2.2 Background Slope Simulations	62
	3.2.3 Minnaert Analysis	62
	3.2.4 Summary	69
4.0	CONCLUSIONS AND RECOMMENDATIONS	71
	REFERENCES	74
	APPENDIX A	76

LIST OF FIGURES

Figure		Page
1	Hypothetical plots of $S = So \cos^{\kappa}(i)$ for $\kappa = .5$, $\kappa = 1.0$, and $\kappa = 1.5$	12
2	Scatter plot of normalized sensor response versus cos (i) for forest opening data acquired in August 1976	13
3	Scatter plot of normalized sensor response for Leadville snow data	15
4	Scatter plot of normalized sensor response versus cos (i) for lodgepole pine data acquired in August 1976	16
5	Scatter plot of normalized sensor response versus cos (i) for Leadville lodgepole pine data acquired in May 1978	18
6	Scatter plot of irradiance values measured by aircraft sensor versus time of day	29
7	Flightline and point locations for files 6 and 7 . . .	31
8a-c	Minnaert plots of lodgepole data for files 6 and 7, channels 1, 2 and 3	32
9	Diagram of geometric relationships between sun and sensor position	38
10	Horsetooth, Colorado study site	42
11	Minnaert plots of Landsat MSS data for ponderosa pine	45
12	Minnaert corrected and uncorrected Landsat MSS data versus cosine of solar incident angle	48
13	Lambertian corrected Landsat MSS data versus uncorrected Landsat data	50
14	Minnaert corrected Landsat MSS data versus uncorrected Landsat data	51
15	Simulated and measured reflectance of a one-layered lodgepole pine canopy for July 1, 1977	57

Figure		Page
16	Simulated and measured reflectance of a three-layered lodgepole pine canopy for July 1, 1977	58
17	Simulated and measured reflectance of a Russian olive tree for August 9, 1978	60
18	Simulated and measured reflectance of a grass canopy (*Agropyron sp.*) for May 18, 1978	61
19	Normalized reflectance versus slope for Russian olive at two wavelengths	63
20	Normalized reflectances versus slope for lodgepole pine at two wavelengths	64
21	Minnaert plots of simulated Russian olive response in two wavelengths	65
22	Minnaert plots of simulated lodgepole pine response in two wavelengths	66
23	Normalized response versus cos e for Russian olive simulated at wavelengths of .68 and .80 μm . . .	67
24	Normalized response versus cos e for lodgepole pine simulated at wavelengths of .68 and .80 μm . . .	68

LIST OF TABLES

Table		Page
1	Descriptions of sun angle experiments by site, date, terrain type, solar zenith angle, and sky conditions	8
2	Summary of sun angle experiment regression analysis for Leadville M-3 and CSFS sites	10
3	Catalog of radiometric and video data for Leadville, Colorado, July 1, 1978	22
4	Summary of regression analysis for lodgepole pine data at 1:20,000 scale and 12 acre resolution	27
5	Summary of topographic and radiometric data for files 6 and 7	35
6	Summary of regression analysis for files 6 and 7	35
7	Minnaert regression relationships for each Landsat MSS channel	49
8	Linear R^2 values for regression of Landsat MSS channels versus cos i (Lambertian assumption) and for the Minnaert relationship	49
9	T-table for two cases of lodgepole pine and Russian olive at two wavelengths	70

1.0 INTRODUCTION

This is the second of a two volume final report series for the U.S. Forest Service Cooperative Study CA-16-741 entitled "Signature Studies for Natural Resource Inventory." Volume I describes our work under Objective I--Middle Park Inventory Analysis. Volume II discusses our continuing efforts at evaluating the effects of extrinsic variables such as solar illumination and terrain geometry on the recorded spectral character of wildland terrain features. In addition, our progress with incorporating these effects into the Colorado State University Solar Radiation Canopy Reflectance Model are reported.

The objectives of this work were to:

1) Enlarge the existing digitized spectral reflectance data base to include additional vegetation types and second year replication;
2) Evaluate the effects of illumination and terrain geometry on recorded spectral response for various scenes;
3) Develop a process oriented canopy reflectance model sensitive to different sensor/scene parameters;
4) Utilize the model for evaluation and guidance of signature studies for application to scene stratification or signature extension.

In order to achieve these objectives we continued to gather field data from aerial tramways at Leadville, Colorado and at a new site near the Colorado State University Foothills campus located at the Colorado State Forest Service Nursery (CSFS). Aircraft radiometric observations were made over Leadville in cooperation with the U.S. Forest Service and Landsat multispectral data were analyzed from the CSFS site. Those

data enabled us to make quantitative evaluations of the Lambertian scattering assumption for natural resource targets and to guide our modeling efforts. In those cases where the angle between the sun, the dominant illumination source, and the sensor was constant, the Minnaert relationship (1941) proved to be a convenient mechanism for summarizing terrain geometric effects.

This report is organized as follows: Chapter 2.0 describes the extrinsic terrain geometric effects involving the sun, sensor, and surface relationships. Specifically, analysis of field data, aircraft measurements, and Landsat observations are discussed. Chapter 3.0 summarizes our canopy reflectance modeling analysis. This includes model modification benchmark runs, topographic variations, and the Lambertian assumption. Overall conclusions and recommendations are given in Chapter 4.0.

2.0 EXTRINSIC GEOMETRICAL EFFECTS

Much of the work in remote sensing to classify features on the earth's surface has started with the assumption that most natural features interact with electromagnetic radiation according to Lambert's cosine law:

$$I = I_o \cos \theta$$

where: I is reflected intensity

I_o is the intensity of incident radiation

θ is the angle of incidence from the perpendicular

Several authors, however, have reported a dependence of reflected light on sensor and illumination geometry that departs from this relationship (Kriebel, 1978; Duggin, 1977; Proctor et al., 1972; Smith and Oliver, 1974; Stewart, 1971; and Monteith and Szeicz, 1961).

We have attempted to quantify this phenomenon in terms of an empirical photometric function proposed by Minnaert (1941) and later given the distinction Minnaert's "Law". This function is described as:

$$B_s (\lambda, \alpha, i, e) = B_n (\lambda, \alpha) \cos^{k(\alpha, \lambda)} i \cos^{k(\alpha, \lambda)-1} e \qquad (1)$$

where: B_s = measured surface brightness or relative radiance,

B_n = effective normal surface relative radiance,

λ = wavelength,

α = phase angle as measured from sun to sensor,

i = solar incidence angle measured from the surface normal,

e = sensor view angle measured from the surface normal, and

k = Minnaert constant or surface roughness coefficient. K = 1 implies a Lambertian surface.

The above equation may be simplified by:

1) evaluating each wavelength separately,

2) maintaining a constant phase angle α, and

3) multiplying each side of equation (1) by cos e to obtain

$$B_s \cos e = B_n \cos^k i \cos^k e$$

or

$$B_s \cos e = B_n (\cos i \cos e)^k \qquad (2)$$

This function has received widespread use in the field of astrophysics to determine the surface characteristics of planetary bodies (Veverka et al., 1978; Young and Collins, 1971; and Hapke and Van Horn, 1963) as examples. Its application to terrestrial remote sensing, however, has been limited (Gillespie and Kahle, 1977).

A convenient method for evaluating the surface characteristics of a terrain type in terms of the effects of illumination and geometry is to use the Minnaert function in logarithmic form. Taking the Log of both sides of equation (2) we have:

$$\text{Log } B_s \cos e = \text{Log } B_n + k \cos i \cos e \qquad (3)$$

The equation is not in a linear form and a least squares line may be fitted to the observed values to obtain estimates of k and B_n. Log B_s cos e is the "response" variable and log cos i cos e is the variable. Fitting a line to the data gives the intercept (log B_n) and slope coefficient k. B_n is the spectral radiance value for a particular surface type that a sensor would measure if both the sensor and sun were located at the slope normal position. In practice it is also sensitive to sensor calibration factors. This is equivalent to a horizontal

surface with the sun and sensor at the zenith. k describes the nature of the angular scattering response. A Lambertian surface yields $k = 1$, whereas specular components give rise to larger or smaller k values.

It is convenient to represent most natural surfaces according to the Minnaert function. Where all of the variables except k and B_n are quantified or limited in range, regression analysis may be used to determine predicted values of the coefficient for particular scene types. Most remote sensing work has assumed that terrain surfaces will behave as Lambertian diffuse reflectors. This is known to be incorrect for many cases and may be tested by use of the Minnaert relationship.

Caution must be exercised in applying the Minnaert function, however, since it may be sensitive to the ratio of direct to diffuse irradiance and the phase angle.

We have used this technique to analyze the illumination and terrain geometry effects on sensor response from three remote sensing systems. The first was the tramway mounted Scene Recording Radiometer (SRR) at the Leadville M-3 and the CSFS study sites. The second was a four channel aircraft mounted radiometer system developed by the U.S. Forest Service and used over the Leadville vicinity. The third system was Landsat MSS data recorded over the Horsetooth, Colorado area.

2.1 Data Acquisition for 1977-78

Our data collection efforts for this contract year emphasized expanding our spectral data base for logepole pine to include measurements at different times of the year and establishing a new study site over a tall grass community near Fort Collins. This latter site also contained some deciduous trees. A new scene recording radiometer (SRR-II)

was completed and tested which provides for measurement of narrow band irradiance adjacent to narrow band scene radiance measurements.

Reflectance measurements at the Leadville M-3 test site were made on July 1, July 11-12, August 24, October 14, 1977 and May 23-25, 1978. Additional data were acquired for the IH-1 site on August 14, 1977.

A new study site was established at the Colorado State Forest Service Nursery in October, 1977 in conjunction with the U.S. Army Corps of Engineers Waterways Experiment Station. A 45.7 m (150 ft) tramway was constructed with 9.1 (30 ft) support towers. This provides a nominal field of view of 3.7 m (12 ft) on the ground. The site is characterized by several grass species including *Festuca sp.*, *Poa sp.*, *Carex sp.*, *Agropyron sp.*, and *Bromus sp.* Several small Russian olive (*Eleaegnus angustifolia*) trees are also located within the transect. Spectral reflectance measurements at this site were conducted on December 16, 1977, April 20, and May 18, 1978. The data acquired on May 24 at Leadville and April 20 and May 18 at the CSFS Nursery were from experiments designed to evaluate the effects of changing sun angle on recorded scene spectral characteristics. The results of these experiments and two others conducted in August, 1976 are discussed later.

In addition, data from the July, 1977 U.S. Forest Service aircraft overflight of the Leadville area were reduced and analyzed as discussed in a subsequent section. An August 15, 1972 Landsat image of the CSFS site was also analyzed.

2.2 Aerial Tramway Sun Angle Experiments--Constrained View Angle and Topography Case

Our tramway mounted SRR data acquisition system provides a convenient way to evaluate the surface properties of various terrain types. The

SRR can be positioned over a scene and the radiance measured in six spectral bands at various times of day. For these experiments the view angle was normal to the surface (e = 0) and the phase angle (α) is equivalent to the solar zenith angle ($\alpha = i$). The Minnaert relationship discussed earlier usually requires a small range of α values. When this condition is not met, it can still be used to test for Lambertian behavior. However, given the large quantity of field data available and the obvious non-Lambertian trends, the authors decided to employ Lambert's Law directly to evaluate the effect of sensor response as a function of changing illumination angle (i).

Using this relationship we examined data collected at different times of the year at Leadville and the CSFS Nursery sites for three terrain types. Descriptions of these experiments are included in Table 1.

2.2.1 Experimental Procedures

The data collection procedures for these experiments consisted of establishing the scene location, recording scene radiance in six spectral bands, acquiring narrow and broad band irradiance and obtaining periodic photographs of the scene. These procedures are described in detail by Berry, Heimes and Smith (1978) and Heimes and Smith (1977). The detector signal recorded for these experiments is a relative measure of scene spectral response and was not converted to absolute units.

The relationship used in this analysis can be written as:

$$S(\lambda) = S_n \cos^{\kappa} i(\lambda, \alpha)$$

where S is the recorded sensor response as a function of wavelength and S_n is the expected sensor response normal to the surface (i. e., $i = 0$). The exponent κ varies with the wavelength and phase angle

Table 1 . Descriptions of sun angle experiments by site, date, terrain type, solar zenith angle range, and sky conditions. Percent diffuse solar radiation is shown in parenthesis. N = number of observations.

Site	Date	Terrain Type	Solar Zenith Angle Range	Sky Conditions	N
Leadville	Aug. 4, 1976	Lodgepole pine	69-20	Clear to partly cloudy (N.A.)*	22
	Aug. 6, 1976 (a.m.)	Forest opening	57-22	Clear to partly cloudy (N.A.)*	16
	Aug. 6, 1976 (p.m.)	Forest opening	23-45	Partly cloudy (N.A.)*	11
	May 24, 1978 (a.m.)	Lodgepole pine	79-19	Clear (≃5%)	23
	May 24, 1978 (a.m.)	Forest opening	78-19	Clear (≃5%)	23
CSFS	April 20, 1978 (a.m.)	Tall grass	55-30	Hazy, cloudy (≃14%)	11
	April 20, 1978 (p.m.)	Tall grass	31-63	Hazy, partly cloudy Hazy, clear, cloudy (≃18%)	11
	May 18, 1978 (a.m.)	Tall grass	38-21	Partly cloudy, clear (≃8%)	9
	May 18, 1978 (p.m.)	Tall grass	22-83	Partly cloudy, overcast, partly cloudy, clear (≃26%)	19

*Diffuse/Direct data was not available.

and the reflection properties of the surface. The objective of this analysis was to determine if the effect of changing illumination angles on sensor response was a linear relationship. If this is the case than an estimated slope coefficient would be valid for a certain range of i values, assuming, of course, no change in atmospheric quality.

The data were prepared for evaluation by calculating the solar zenith angle for each observation and taking the logarithms of the recorded radiances in each band and the coincident zenith angles for each experiment. The data were analyzed using an interactive statistics package available on the Colorado State University CYBER 171 and 172 computers called MINITAB (Ryan, Joiner and Ryan, 1976). This program allows data to be input from mass storage and manipulated in various ways. The logarithmic transformation was performed within MINITAB. Linear regressions were conducted with the logarithm of the cosine of the zenith angle (cos(i)) being the independent variable.

2.2.2 Experimental Results

After preliminary results were obtained a noticeable difference in estimated slope coefficients between morning and afternoon data was observed for the same day. It was then decided to stratify the experiments into morning and afternoon populations. The regression results for all experiments are summarized in Table 2 for each spectral band. From this table it is apparent that the slope coefficient κ may vary from morning to afternoon for the same scene. Also, κ appears to be wavelength dependent. The correlation coefficients for the regressions ranged from .54 to .98 with the majority falling in the .80 to .95 range indicating a significant amount of the variation is a function of the

Table 2 . Summary of sun angle experiment regression analysis for Leadville M-3 and CSFS sites. Spectral bands 1-6 for Aug 1976 data are 480nm, 514.5nm, 550nm, 675nm, 800nm, and 960nm respectively. Spectral bands for all 1978 data are 480nm, 550nm, 680nm, 730nm, 800nm, and 960nm respectively. LP = Lodgepole pine, FO = Forest Opening, AM = Morning (decreasing zenith angle), PM = Afternoon (increasing zenith angle). Standard deviations of slope coefficients are enclosed in parentheses.

		Slope Coefficient (K) Spectral Band						Coefficient of Determination Spectral Band					
Site	Date	1	2	3	4	5	6	1	2	3	4	5	6
Leadville LP	Aug 4, 1976 (AM)	2.75 (.14)	2.56 (.13)	2.45 (.12)	2.52 (.15)	1.93 (.08)	2.30 (.08)	.95	.95	.95	.93	.97	.98
Leadville FO	Aug 6, 1976 (AM)	1.50 (.08)	1.15 (.07)	1.52 (.09)	1.52 (.08)	1.06 (.06)	1.13 (.08)	.96	.95	.95	.96	.96	.94
Leadville FO	Aug 6, 1976 (PM)	1.45 (.19)	1.11 (.19)	1.56 (.22)	1.61 (.21)	1.08 (.19)	1.23 (.18)	.85	.76	.83	.85	.76	.82
Leadville LP	May 24, 1976 (AM)	1.68 (.18)	1.39 (.10)	1.58 (.16)	.95 (.04)	.85 (.04)	1.01 (.03)	.80	.89	.82	.96	.96	.98
Leadville Snow	May 24, 1978 (AM)	1.44 (.07)	1.35 (.05)	1.29 (.06)	1.25 (.05)	1.17 (.04)	1.33 (.17)	.96	.97	.96	.97	.98	.77
CSFS Grass	April 20, 1978 (AM)	.83 (.08)	.82 (.14)	.80 (.21)	.52 (.06)	.46 (.07)	.43 (.08)	.92	.77	.58	.86	.79	.73
CSFS Grass	April 20, 1978 (PM)	2.60 (.21)	2.44 (.24)	2.46 (.28)	2.49 (.30)	2.38 (.32)	2.86 (.36)	.93	.89	.87	.85	.82	.84
CSFS Grass	May 18, 1978 (AM)	2.56 (.17)	2.12 (.09)	2.33 (.09)	1.50 (.14)	1.40 (.19)	1.71 (.22)	.97	.98	.97	.93	.87	.89
CSFS Grass	May 18, 1978 (PM)	1.80 (.11)	1.64 (.09)	1.68 (.04)	1.28 (.15)	1.23 (.09)	1.59 (.06)	.93	.95	.99	.79	.92	.97

solar zenith angle. Because of the wide range of κ for similar terrain types it is not evident that this analysis provides an absolute measure of the slope coefficient for a particular surface.

The results of the sun angle experiments, however, can provide a qualitative description of how a particular surface compares to the idealized case of Lambertian response. Referring to Figure 1, the function of:

$$I = I_o \cos^{\kappa} i$$

is plotted for $\kappa = 1.0$, the Lambertian case, and $\kappa = .5$ and 1.5 for theoretical non-Lambertian situations. Similar plots can be made using empirical data and comparisons made between the empirical and predicted curves. This was done for the M-3 forest opening for August and snow covered May data and for lodgepole pine data acquired in August and in May.

Figure 2 shows the plots of normalized responses versus $\cos(i)$ for the August forest opening in the .68 μm and .80 μm wavelength bands. The sensor response data was normalized to the intercept value for $\cos(i) = 1$ from the previous regression analysis. This normalizes the data over the entire range rather than over a single maximum. The values for a theorized Lambertian surface are plotted as a solid line for comparison purposes. For these data the .80 μm responses follow the Lambertian case within the range of .56 to .92 for $\cos(i)$ values and 56° to 23° for solar zenith angle. The response values for the .68 μm band show a definite linear trend with a different slope than the Lambertian case indicating non-Lambertian behavior in this highly absorptive band.

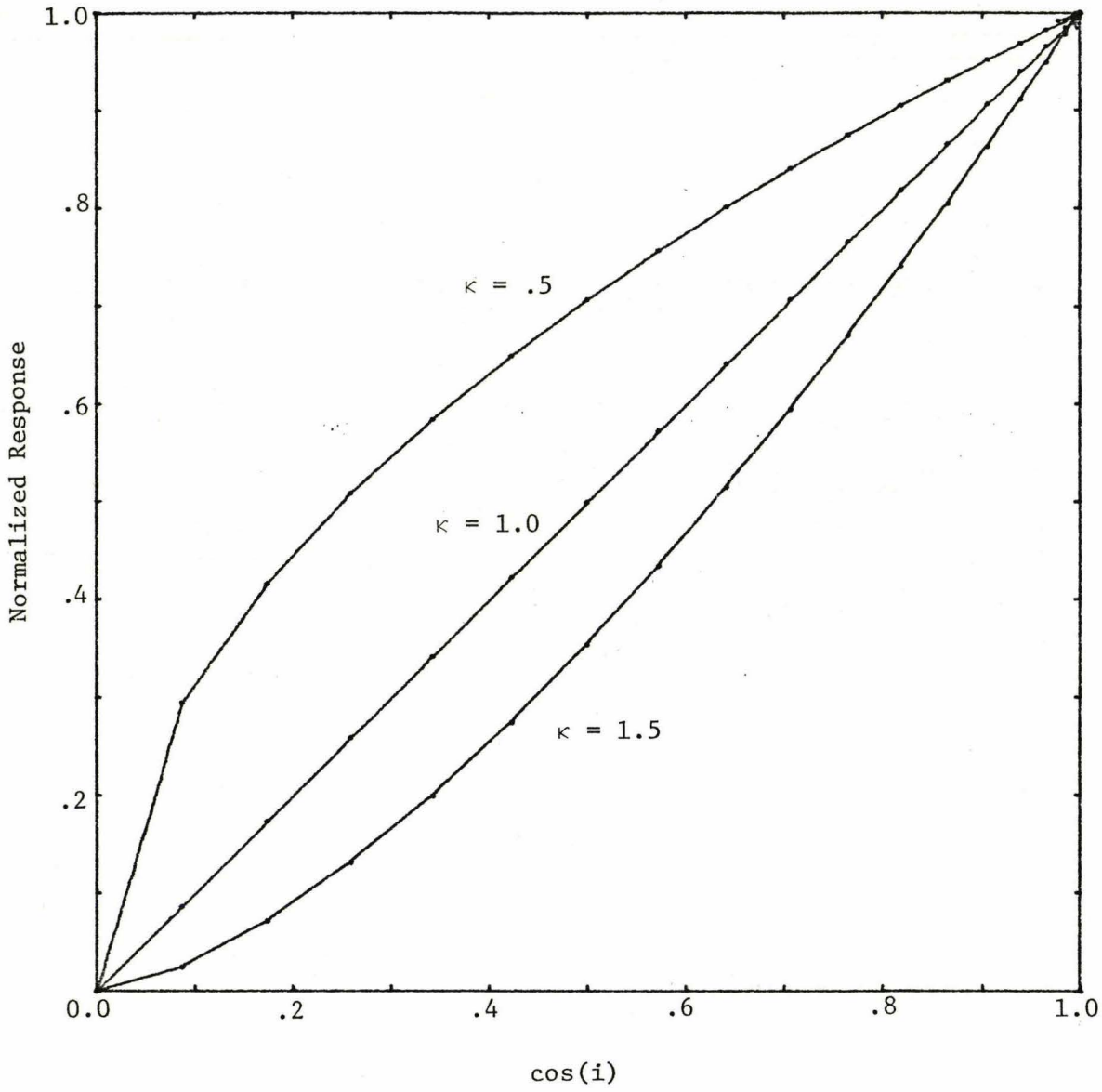

Figure 1 . Hypothetical plots of $S = S_o \cos^{\kappa}(i)$ for $\kappa = .5$ $\kappa = 1.0$ and $\kappa = 1.5$.

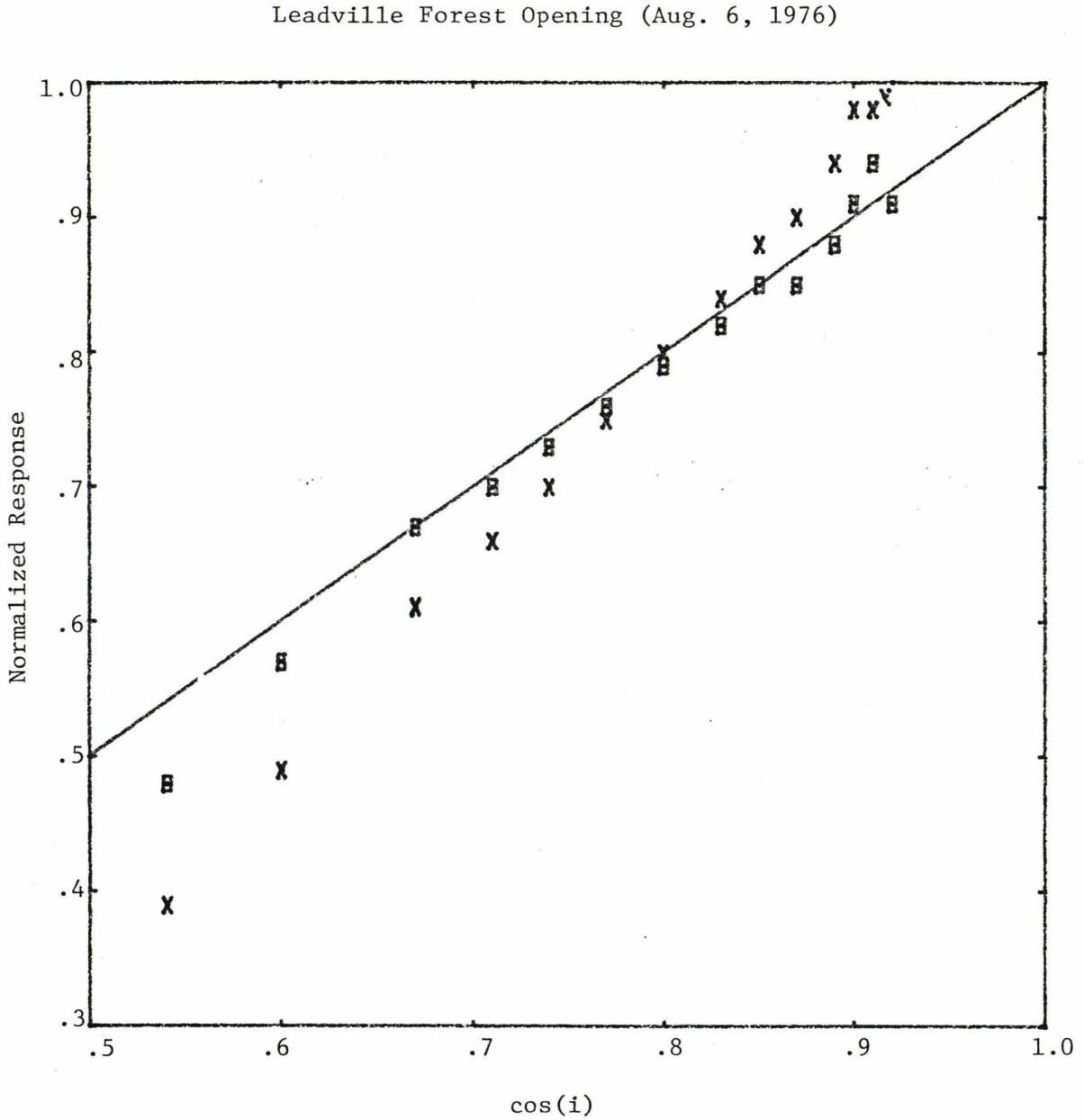

Figure 2 . Scatter plot of normalized sensor response versus cos(i) for forest opening data acquired in August, 1976. i = solar zenith angle, x = 680 μm response data, 0 = 800 μm response data. Solid line indicates Lambertian response.

The May snow covered forest opening data is plotted in Figure 3. A similar method was used to normalize the .68 μm and .80 μm response data. In this case data for the .80 μm band tends to parallel the predicted Lambertian line between .48 and .90 cos(i) values or 61 to 26° solar zenith angle. The .68 μm band data appears to have a slightly different slope in this case, but deviates in the opposite direction from the August data. In both bands the values tend to diverge around 66° and 22° zenith angles. The downward shift of the normalized responses from the predicted line may be more a function of the normalization procedure than displacement due to the surface characteristics. This is due to a rapid increase in sensor signal observed between solar zenith angles of 20 to 0°. The values reported for κ for this experiment in Table 2 show general agreement with those of Veverka (1973) who evaluated the Minnaert Constant of κ as a function of various phase angles from in site snow measurements.

The trend of lodgepole pine data acquired in August, 1976 is shown plotted in Figure 4. The target consisted of a clump of lodgepole pines with some understory grasses occurring within the field of view. The plots for the .68 μm and .80 μm data appear to behave as a $\cos^{\kappa} i$ function with $\kappa > 1$, however, the .80 μm plots exhibit a linear trend for cos(i) values between .4 and .8 or solar zenith angles of 66 to 37°. The slope within this range tends to parallel that for the Lambertian case. The .68 μm data shows a linear trend between .5 and .8 cos(i) values or 60 to 37° solar zenith angle. Within this range the slope parallels that of the Lambertian case. In both cases a rapid increase in response occurs at solar zenith angles less than 29°.

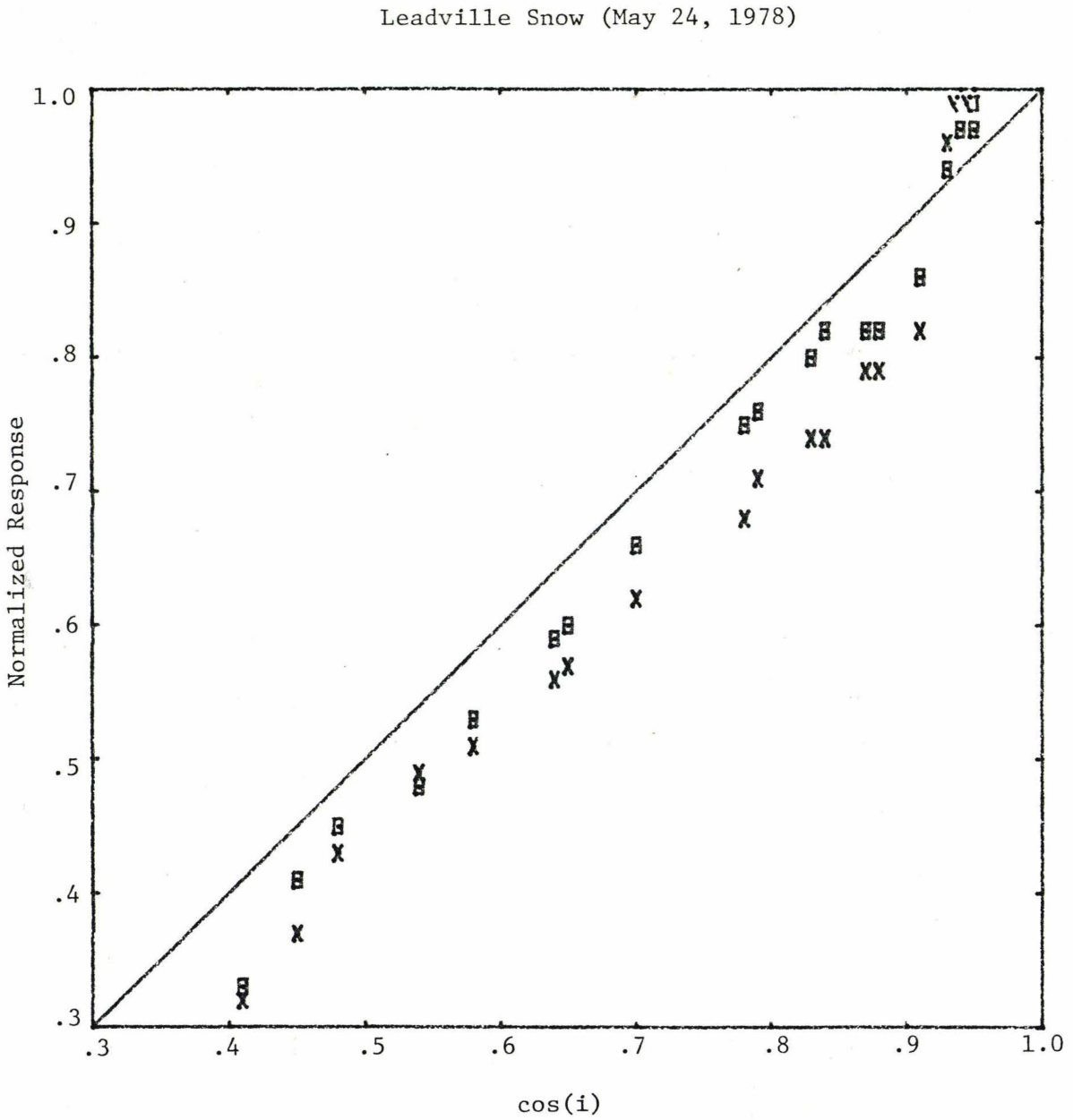

Figure 3 . Scatter plot of normalized sensor response versus cos(i) for Leadville snow data. i = solar zenith angle, x = 680 μm response data, 0 = 800 μm response data. Solid line indicates Lambertian response.

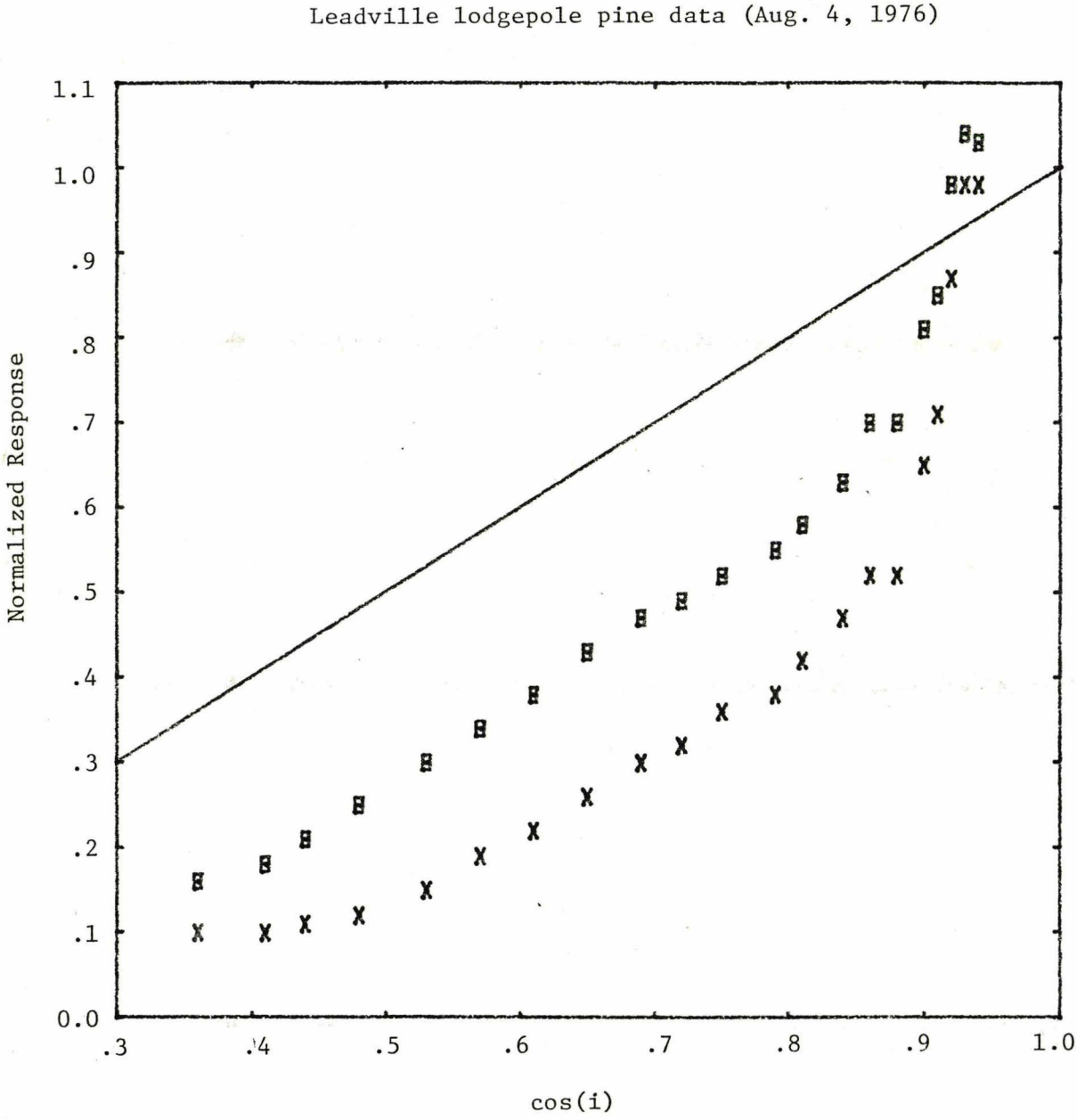

Figure 4. Scatter plot of normalized sensor response versus cos (i) for lodgepole pine data acquired in August, 1976. i = solar zenith angle, x = .68 μm response data, Θ = .80 μm response data. Solid line indicates Lambertian response.

Finally, the data for the experiment conducted in May, 1978 is presented in Figure 5. The target consisted of a cluster of lodgepole pines located adjacent to the meadow opening. The tree canopies covered the FOV except for about 10% on one edge that contained snow covered understory. The plot of .80 μm data shows a linear trend between cos(i) values of .2 and .8 or zenith angles of 78 to 37°. The slope of this range of data is only slightly different than that of the predicted Lambertian case. The .68 μm data, however, shows more scatter with a slope that does not follow the Lambertian case. Again the response values in both bands increase rapidly toward solar noon.

2.2.3 Summary

Results from the analysis of the four experiments show definite trends with respect to cos(i). First of all, the near infrared band (.80 μm) data show a Lambertian-like trend for grassy understory, snow, and lodgepole pine. The .68 μm data appear to deviate from Lambertian behavior for grassy understory and lodgepole pine and parallel the predicted Lambertian line for snow. This may be expected due to the strong absorption of .68 μm light by photosynthetically active plant canopies. All of the Leadville M-3 data showed a rapid increase in response as the solar zenith angle decreased past about 35°. Overall, the plots of normalized response versus cos(i) indicate that a linear trend exists within various ranges of phase angles. Further analysis may provide insight to the optimum range of illumination angles for discriminating certain terrain types. Preliminary studies show that slopes remain stable over a range of solar zenith angles from 53° to 46° for data acquired during morning hours.

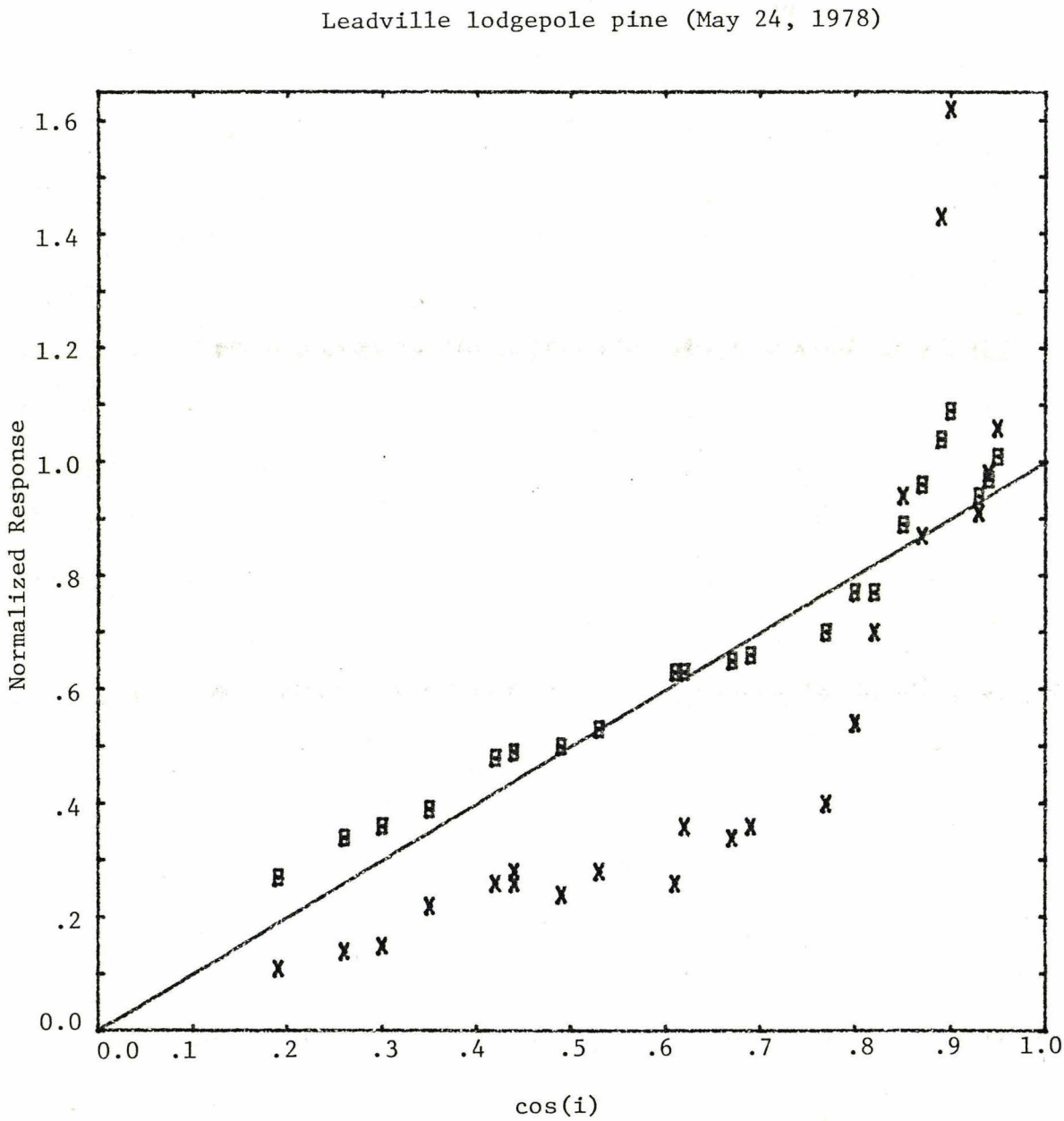

Figure 5. Scatter plot normalized sensor response versus cos (i) for Leadville lodgepole pine data acquired in May, 1978. i = solar zenith angle, x = .680 μm response data, θ = .800 μm response data. Solid line indicates Lambertian response.

2.3 Analysis of Topographic Effects on Airborne Radiometer Data

Data collected by an airborne radiometer spatially registered with a vidicon camera offers a means to evaluate topographic influences on scene spectral response. Spectral radiance values measured by a remote sensor vary with sun angle, i, view angle, e, and phase angle, α. Sun angle and view angle are measured with respect to the normal vectors of the observed surface and consequently vary greatly with changing terrain slopes and aspects. Phase angle is defined as the angle between solar position and sensor position. For narrow fields of view and short time intervals, phase angle is fairly constant. The Minnaert relationship as discussed previously in this report conveniently summarizes the geometrical orientation of sun, sensor, and terrain. Analysis of the aircraft data has utilized this relationship in the attempt to establish limits for topographic variability of radiance for certain terrain types.

2.3.1 Instrumentation

The Rocky Mountain Forest and Range Experiment Station at Fort Collins, Colorado, has assembled instruments for use in a twin engine aircraft (Aldrich, et al., 1977). These include a four channel radiometer, a video camera and recorder, an irradiance meter, a digital data logger, and D/C to A/C power inverter. A 70 mm. camera is used for photographic coverage.

The radiometer has a field of view of 9.4 degrees and is optically boresighted for spatial registration between spectral channels. It is rigidly mounted with the video camera so that measurements and pictures are of virtually the same spot on the ground. Filters for spectral separation may be matched to the Landsat multi-spectral scanner, or

chosen for special characteristics desired. Narrow band interference filters bandpass centered at 480 nm, 550 nm, and 680 nm were used for this study.

The irradiance meter consists of a diffusing receptor mounted on the top surface of the aircraft, a fiber optic light guide, and a filter wheel radiometer for wavelength separation and detection. The irradiance meter and video camera were both filtered for MSS band 5 (600 nm to 700 nm).

The radiometer and irradiance meter provide analog signals that are sampled once every second by the data logger. Measurements are recorded on computer compatible tape along with a time code from a digital clock. A video clock module displays elapsed time in the corner of the picture frame in minutes, seconds and hundredths of seconds. The two clocks are manually synchronized so that a particular measurement may be associated with an image of the scene.

2.3.2 Study Site

The site is located near the town of Leadville, Colorado. Most of the measurements are of the Iron Hill and Evans Gulch areas to the east, however, three of the twelve flight lines extend westward to Turquoise Lake. The area involved is about twelve miles in the east-west direction by four miles north and south. Elevations range from about 9,900 ft (3018 m) at Turquoise Lake to nearly 12,000 ft (3658 m) at Prospect Mountain. There is a full range of aspect angles (from 0° to 360°) and slopes range from 0° to about 25°.

The Iron Hill site is the location of the tower and tramway system used in Section 2.2 and earlier research (Heimes and Smith, 1977).

On July 1, 1977, a total of twelve measurement passes were made over portions of the study site between 10:45 and 11:50. Six of these passes were obtained at 5000 ft (1524 m) above the terrain, and six at 1000 feet (305 m). Since the 9.4 degree field of view of the radiometer is fixed, spot size at the 5000 foot (1524 m) level is 818 feet (250 m) in diameter or about 12 acres (4.9 ha); while at 1,000 feet resolution is 164 feet (50 m) or .48 acres (.2 ha). Each pass resulted in one file of information being recorded by the data logger. Files 1, 2, 3, 5, 6 and 7 were made at 5000 feet, while files 9, 10, 11, 12, 14, and 15 were at 1000 feet. Files 4, 8, 13, and 16 were recorded with the radiometer lenses covered to establish a no energy or "zero" voltage level for the detector electronics. During the mission, the 800 nm channel was turned off due to malfunction of the recording electronics. As a result, data for only the 480 nm, 550 nm and 680 nm channels were recorded.

2.3.3 Data Reduction

Available information for this study consisted of: 1) a computer compatible tape of clocktime, irradiance, and three channel radiance, (the U.S. Forest Service provided a listing of all the data values for the sixteen files of information consisting of 12 measured passes and 4 zeroing runs), 2) a video tape display of flightlines and elapsed time, 3) photographic coverage at 1:20,000 and 1:4,000, and 4) United States Geologic Survey topographic maps at 1:24,000. Table 3 lists the radiometric and video data analyzed in this study.

By viewing the video tape and locating recognizable features such as roads, mines and ponds, all flight lines were mapped at 1:24,000 and annotated with elapsed time from the video display. From the flight lines and the radiometer listing, a catalog of file number, flight

Table 3. Catalog of radiometric and video data acquired over Leadville, Colorado on July 1, 1977.

File #	Flight Line	Radiometer Clock (Mtn. Daylight Time)	Video Clock	Video Recorder Footage
		10:45:00	4:00	000
1	1-1	10:45:11 10:47:10	4:11 6:10	003 033
2	2-1	10:51:13 10:53:10	10:13 12:10	047 077
3	3-1	10:58:51 11:02:49	2:51 6:49	100 166
5	3-2	11:05:09 11:07:47	9:09 11:47	204 253
6	1-2	11:14:28 11:15:46	4:28 5:46	257 282
7	2-2	11:18:27 11:19:45	8:27 9:45	284 310
9	1-1	11:25:10 11:26:00	2:10 3:00	314 331
10	2-1	11:28:15 11:28:55	5:15 5:55	333 343
11	3-1	11:32:50 11:36:10	9:50 10:32 11:56 13:10	347 361 362 389
12	2-2	11:40:52 11:41:20	17:52 18:20	390 400
14	2-3	11:44:09 11:44:47	21:09 21:47	402 417
15	2-4	11:46:53 11:47:51	23:53 24:51	421 444

File numbers 4, 8, 13, and 16 were used to zero radiometer.

line number and clock time was prepared to facilitate cross references to various data formats. Photographic coverage was also mapped at 1:24,000.

FORTRAN program NORM was provided by the Rocky Mountain Forest and Range Experiment Station to read and decode the computer tape. The output from this program is a listing of raw data values for each of the sixteen files. Because of parity errors with the computer compatible tape and a change of computer operating systems at Colorado State University, it was very difficult to read the complete tape. Typically only two or three good files of data would result from each attempt. For this reason, as good files were obtained they were punched on cards untile the entire set of data was complete.

A program was written to read the "zeroing files" and calculate a mean value for each wavelength channel. The data logger erroneously failed to code a negative sign for several values within the zeroing runs. In calculating means, this omission would have significantly affected the results, so negative values were enforced where necessary. The program output the mean, maximum and minimum range, variance, and standard deviation for each channel. Standard deviations at zero energy level indicated sensor drift of less than one percent for all channels.

Next, files of measurements were read and adjusted by the "zero" values calculated above. Descriptive statistics were calculated and data listings were made. Data lists consisted of radiance (3 channels) and irradiance observations, video display time, clock time and point identifiers (file and point number). Since the irradiance probe was not covered during zeroing runs no adjustment of these values was

possible. Output of the program was to a line printer and to a permanent disk file for later use.

In order to associate radiance values with terrain slope and aspect, sample points from the video display were located as accurately as possible on United States Geologic Survey topographic maps at 1:24,000 scale. Only points on relatively homogeneous slopes whose location was certain were used in analysis. Sixty-nine such points were first located on photographic prints at 1:5,000 scale and transferred to base maps by zoom transfer scope. At 12 acre resolution, points were visually transferred from the video display to the maps using reference points visable on both data sets.

Slope and aspect were determined from topographic maps. Slope (inclination angle) is the arc tangent of the elevation difference divided by the measured horizontal distance after scale conversions were made. Aspect is the azimuth of steepest downward slope measured clockwise from north. Values for slope, aspect and point identifier were stored on permanent disk file.

A program to calculate solar position, cos(i), and cos(e) for each sample point was written. Terrain slope and aspect are read from one file and the time and radiance values from another. Other necessary inputs are site latitude and longitude, and appropriate solar ephemeris values for declination and equation of time.

The angle of incidence (i) is calculated from:

$$\cos i = \sin\Psi_{sun} \sin\Psi_{n} \cos(\Theta_{sun} - \Theta_{n}) + \cos\Psi_{sun} \cos\Psi_{n}$$

Table 4. Summary of regression analysis for lodgepole pine data at 1:20,000 scale and 12 acre resolution.

Channel	No. of Points	K	R^2	$t_{K=1}$
1	47	1.15	.21	.45
2	47	1.24	.25	.76
3	47	1.67	.21	1.40

2.021 is the critical value of t at 95% confidence level

was tested separately to determine intercept (B_n) and slope (k) parameters, along with t-values calcualted for the $k = 1$ null hypothesis.

A test was done for the null hypothesis that $k = 1$. A k value of 1 indicates that a surface is behaving as a uniform diffuse reflector, that is, a Lambertian surface. This is an assumption often made in remote sensing studies. Rejecting the $k = 1$ null hypothesis would allow the conclusion that the surface was non-Lambertian, for the range of incidence and exitance angles present in the data.

The $t(k = 1)$ column in Table 4 lists the calculated t statistics for this hypothesis. At the 95% confidence level, we may not conclude that the surface is other than Lambertian. With less unexplained variability in the data, the estimated coefficient k could be calculated with more certainty and narrower confidence intervals.

Further analysis concentrated on this approach. Since data were collected over about one hour interval, it is possible that illumination was not constant. This could be caused by a decreasing solar path length through the atmosphere as the sun rose towards zenith. Atmospheric attenuation would decrease and consequently, irradiance would increase. It is also possible that the state of the atmosphere was not constant due to varying water vapor or particulate conditions. A plot of the irradiance values measured by the aircraft sensor, versus the time of day should reveal such changes (Figure 6).

Since data points were numbered sequentially as the mission progressed plotting irradiance versus point number should reveal point groups where irradiance did not significantly change. From the plot of the 12 acre resolution lodgepole pine data this was evident. Irradiance

where: Ψ_{sun} = solar zenith angle

Ψ_n = terrain normal zenith angle

Θ_{sun} = solar azimuth angle (clockwise from north)

Θ_n = terrain aspect angle (clockwise from north)

Angle e is determined from:

$$\cos e = \sin\Psi_{sat} \sin\Psi_n \cos(\Theta_{sat} - \Theta_n) + \cos\Psi_{sun} \cos\Psi_n \quad (7)$$

where Ψ_n and Θ_n are as defined above, and

Ψ_{sat} = sensor zenith angle

Θ_{sat} = sensor azimuth angle

If the sensor is at zenith, the previous equation reduces to simply:

$$\cos e = \cos \Psi_n \quad (8)$$

where Ψ_n is also equal to terrain slope angle

For this study the radiometer is assumed to be looking vertically downward from the zenith position, except where the aircraft is banking for a turn, in which case the points are not used. Some tip and tilt of the aircraft no doubt existed, but these could not be accurately quantified from this data set.

2.3.4 Analysis of Sample Points

As explained earlier in this report, solar position, sensor position and topography may be summarized for a given phase angle according to the Minneart relationship described in equation (1).

For the data sets at each resolution level Minnaert plots were made of $LOG[B_s (\lambda, \alpha) \cos e]$ versus $LOG[\cos i \cos e]$. According to the Minnaert hypothesis, if points are from a single surface type, α is constant, and the source of illumination is constant, then the

data points should approximate a straight line with some slope k. Initially, points were not stratified according to vegetation type and density. Under conditions of varying surface type one would not expect the data points to show a significant linear trend, but rather to display a more or less random pattern. That was indeed the result obtained.

Sample points were next stratified according to vegetation type and density. The intention was to group together points where surface appearance and known vegetation were similar. At the 12 acre resolution 47 lodgepole pine points were chosen with an estimated cover density between about 60 and 90 percent. At the half acre resolution, 67 lodgepole pine points of 60 to 90% cover density were identified. Ground truth in the form of black and white photographs was not sufficient to isolate other relatively homogeneous surface types. An attempt to identify a grassy meadow cover type resulted in data indicative of a multipopulation case. Further attempts to isolate suspected populations on the basis of slope, aspect or photo appearance were not successful.

Plots were made for the lodgepole pine surface type at each scale and a regression line was fitted to the data. Output from the regression program was used to test the null hypothesis that the k parameter was equal to 1.0 (The Lambertian case). Rejecting this null hypothesis would allow the conclusion that slope of the Minnaert relationship fitted to the data was some value other than 1. If this occurs, than changes in reflectance geometry caused by varying terrain does affect the radiance values measured by the aircraft sensor.

Table 4 is a summary of the output from the regression program for lodgepole pine data set at 12 acre resolution. Each spectral channel

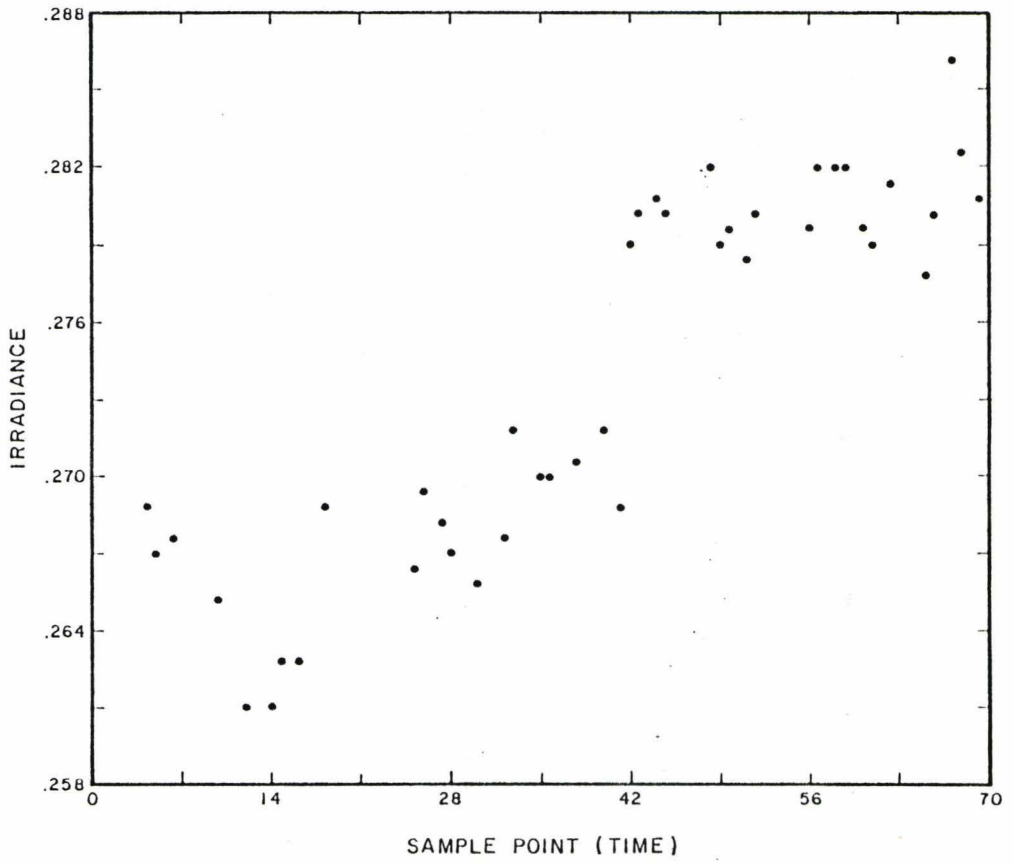

Figure 6. Scatter plot of irradiance values measured by the aircraft sensor versus sample location number.

generally increased through time but was relatively stable for subgrouping of the points. Breaks between subgroups could be associated with file numbers as there was usually a gap of several minutes between files. Examining each file individually, however, reduces the number of points on which to base statistics.

Based on the above considerations, one subgroup of lodgepole pine at the 12 acre resolution was chosen for further evaluation. From point 42 to 69 irradiance was fairly stable as illustrated in Figure 7. These points correspond exactly with files 6 and 7 collected within a period of 5 minutes. This subgroup contains 21 points and should provide a large enough sample to calculate meaningful statistics. Table 5 lists the topographic and radiometric data for this subject. Figure 8 shows the Minnaert plots of the lodgepole data for files 6 and 7.

Increased R^2 values over previous analysis indicates that some additional unexplained variability has been removed (Table 6). Testing the null hypothesis that $k = 1$ does not allow rejection at the 95% confidence level. Again we cannot conclude that the terrain surface has displayed other than a Lambertian response.

At the half acre resolution, a plot of irradiance versus time (or point number) revealed a suspected malfunction of the irradiance meter. Values begin very low, probably at a zero energy response and suddenly increase to a level much higher than previous files of data from a few minutes before (.8 compared to .2). The recorded response of the meter stays at this level for the remainder of the flight with only very small fluctuation, and no general increase with time. Discussions with those researchers who collected the data confirm the possibility of instrument

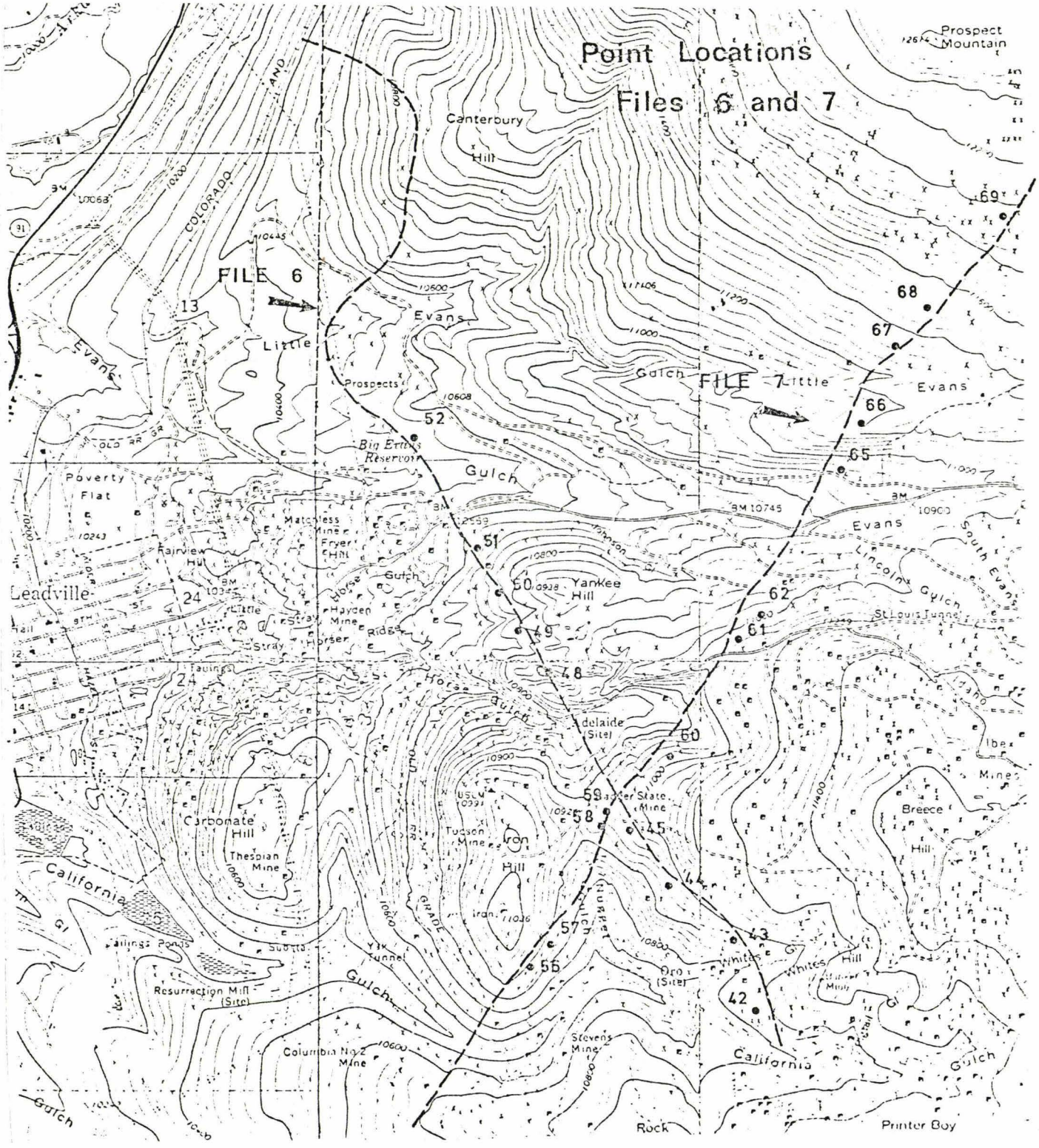

Figure 7. Map of Leadville, Colorado area showing flightlines and sample point locations for files 6 and 7. North is at the top of the map.

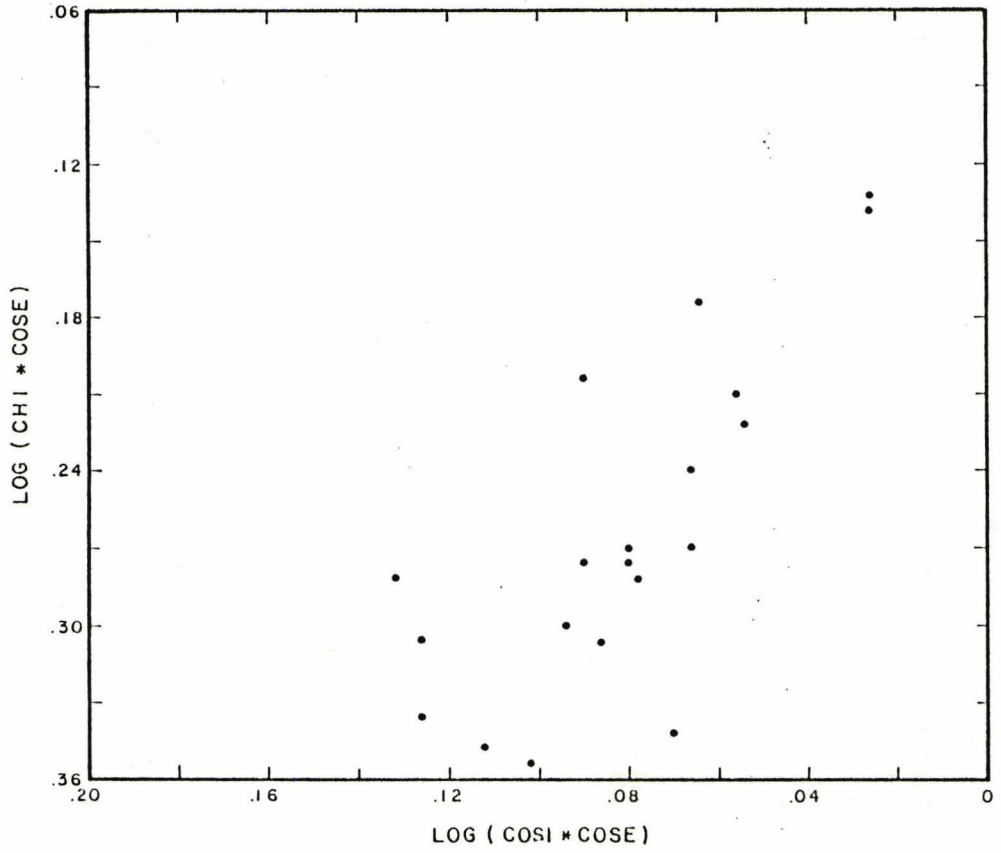

Figure 8a. Minnaert plot of lodgepole data for files 6 and 7 of aircraft radiometer channel 1.

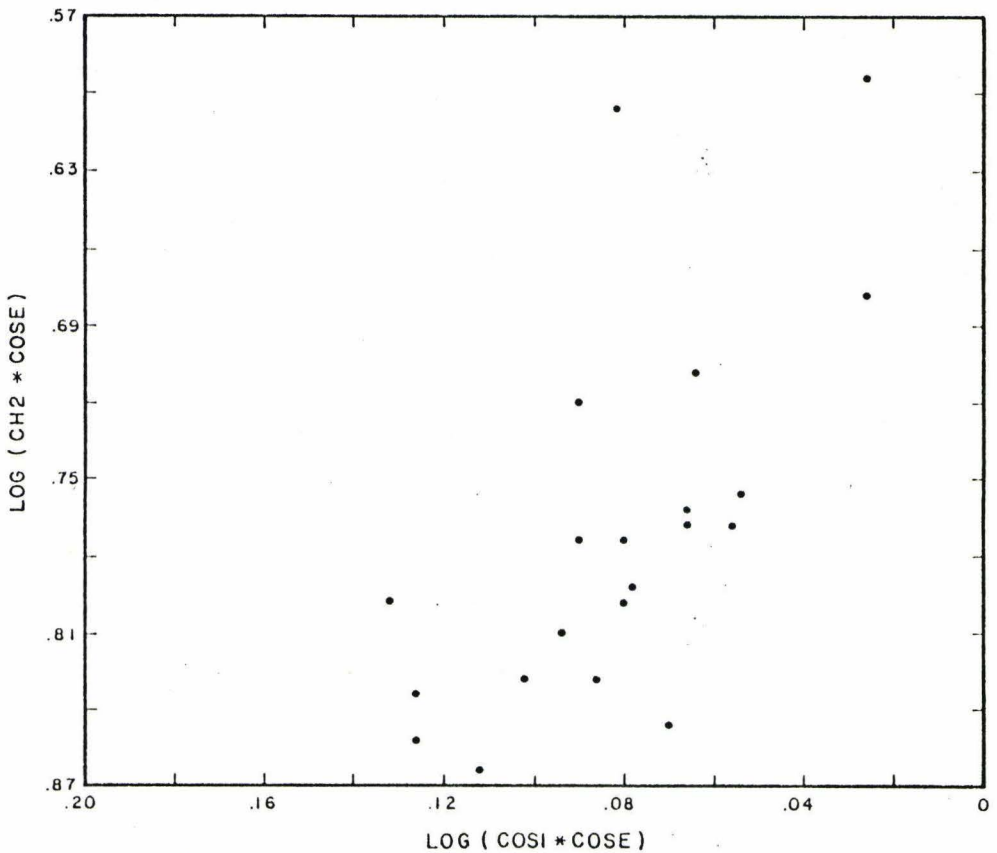

Figure 8b. Minnaert plot of lodgepole data for files 6 and 7 of aircraft radiometer channel 2.

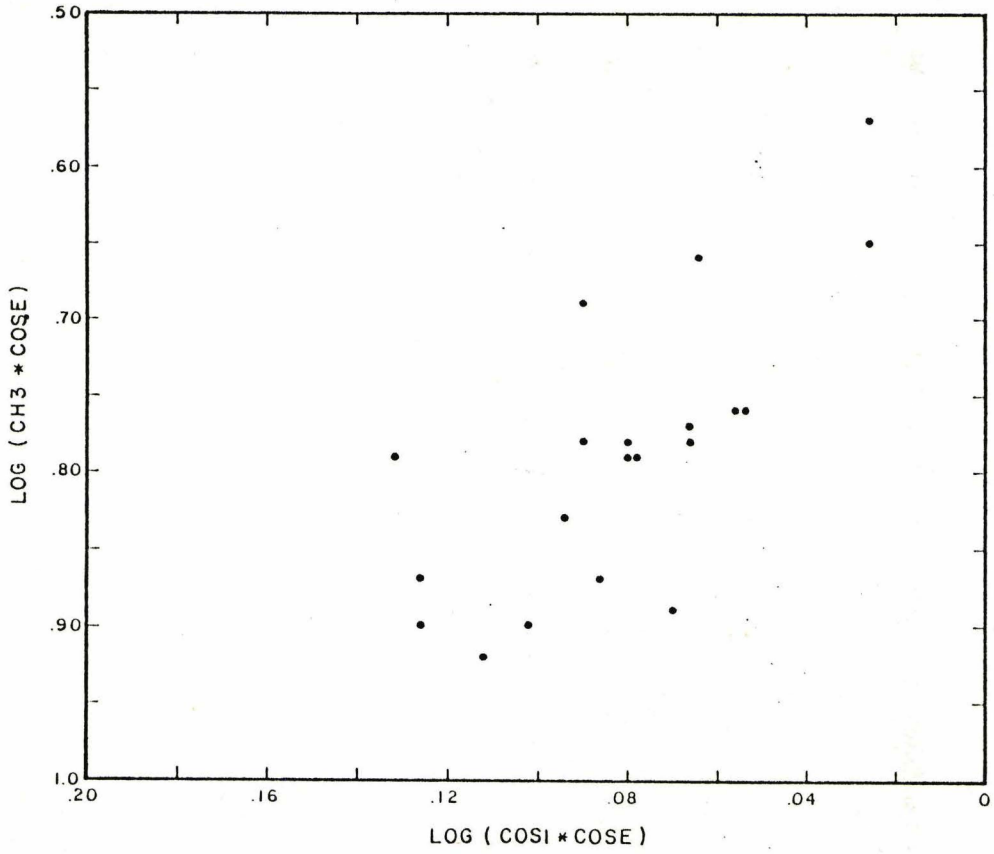

Figure 8c. Minnaert plot of lodgepole data for files 6 and 7 of aircraft radiometer channel 3.

Table 5. Summary of topographic and radiometric data for files 6 and 7.

Sample Number	Slope	Aspect	cos i	cos e	Irradiance	Radiance Ch. 1	Ch. 2	Ch. 3
42	14.0	269.	.76	.97	.278	.541	.164	.165
43	14.0	208.	.86	.97	.280	.536	.166	.167
44	11.0	243.	.82	.98	.280	.511	.157	.149
45	6.8	257.	.84	.99	.280	.538	.170	.169
48	1.3	275.	.88	1.00	.281	.614	.170	.172
49	7.1	264.	.83	.99	.279	.497	.149	.137
50	10.6	271.	.79	.98	.279	.459	.139	.122
51	9.3	283.	.80	.99	.278	.447	.150	.128
52	5.4	230.	.86	1.00	.280	.578	.174	.168
56	17.0	130.	.98	.96	.279	.769	.218	.233
57	15.6	115.	.98	.96	.281	.759	.265	.279
58	4.4	269.	.86	1.00	.282	.536	.170	.167
59	7.6	287.	.82	.99	.282	.536	.170	.167
60	9.8	337.	.82	.99	.279	.628	.193	.207
61	13.4	321.	.77	.97	.278	.477	.145	.128
62	14.0	331.	.77	.97	.281	.506	.151	.139
65	11.9	189.	.90	.98	.277	.611	.178	.176
66	6.2	279.	.84	.98	.280	.543	.160	.165
67	12.3	210.	.87	.98	.286	.465	.146	.130
68	11.3	202.	.88	.98	.282	.684	.201	.224
69	21.0	187.	.89	.93	.280	.912	.267	.317

Table 6. Summary of regression analysis for files 6 and 7.

Channel	No. of Points	K	R^2	$t_{K=1}$
1	21	1.67	.37	1.41
2	21	1.64	.38	1.42
3	21	2.23	.33	1.88

2.093 is the critical value of t at 95% confidence level

error and the unreliability of irradiance values for the half acre resolution set. Consequently, no further analysis were performed on these data.

2.3.5 Summary

The essential conclusion that may be drawn from this study is that for effective zenith sun angles, i, varying from 0 to 40 degrees, and for lodgepole pine canopies of cover intensity greater than 60%, the spectral radiance averaged over a resolution-element of 12 acres (4.9 ha) behaves in a Lambertian manner. That is, we cannot reject the Lambertian hypothesis.

This study has also indicated potential limitations in applying the Minnaert relationship to aircraft scanner data. Small R^2 values for all regressions were obtained. The observations must be grouped into short time intervals in order to insure relatively constant phase angles and atmospheric conditions.

2.4 The Lambertian Assumption and Landsat Data

The Landsat sensors have the capability of acquiring imagery over broad areas with short data acquisition times. Consequently, to a good approximation, the data are obtained under a constant, vertical sensor angle and constant solar illumination angle with respect to the local nadir. That is, the phase angle is constant. If the topography of the scene is flat, all surfaces or materials are also viewed at constant sensor and illumination angles. Effects of directional scattering behavior of the scene surfaces on classification are minimized.

In mountainous terrain, however, the local surface normal varies and consequently a wide range of effective view and illumination angles are obtained, even for a single Landsat image. In these cases

classification of the data is severely impaired (Hoffer, 1974). Several authors have tried various correction procedures to improve the results obtained. These can be broken down into basically empirical approaches which make no assumptions concerning the physical behavior of scene elements and those methods utilizing some assumed natural characteristics of the scene elements (Hart, 1978). Examples of the first approach include channel ratio methods as discussed by Crane (1971 and Vincent (1973). Struve, et al., (1977) gives a detailed explanation of the second approach which assumes Lambertian scattering behavior of the scene elements. This is used to normalize the satellite readings according to the cosine of the effective illumination angle. Topographic slope and aspect for each scene element is required to calculate the effective incidence angle.

Our objectives for the study presented here were to make a rigorous evaluation of the Lambertian assumptions for Landsat data and to examine various recommended correction procedures. We selected a Landsat image of our Colorado State Forest Service study site and employed the Minnaert function to test the Lambertian assumption. A range of effective view angles of 0 to 45 degrees and effective illumination angle of 30 to 80 degrees were present in the data. We restricted out analyses to ponderosa pine (*Pinus ponderosa*) scene elements of similar cover density. If the Lambertian assumption fails to be satisfied for this ideal case, than it would not be expected to apply to more general cases.

2.4.1 Analytical Background

Figure 9 shows the geometrical relationships between the sun, the Landsat satellite, and an arbitrary surface element of slope.

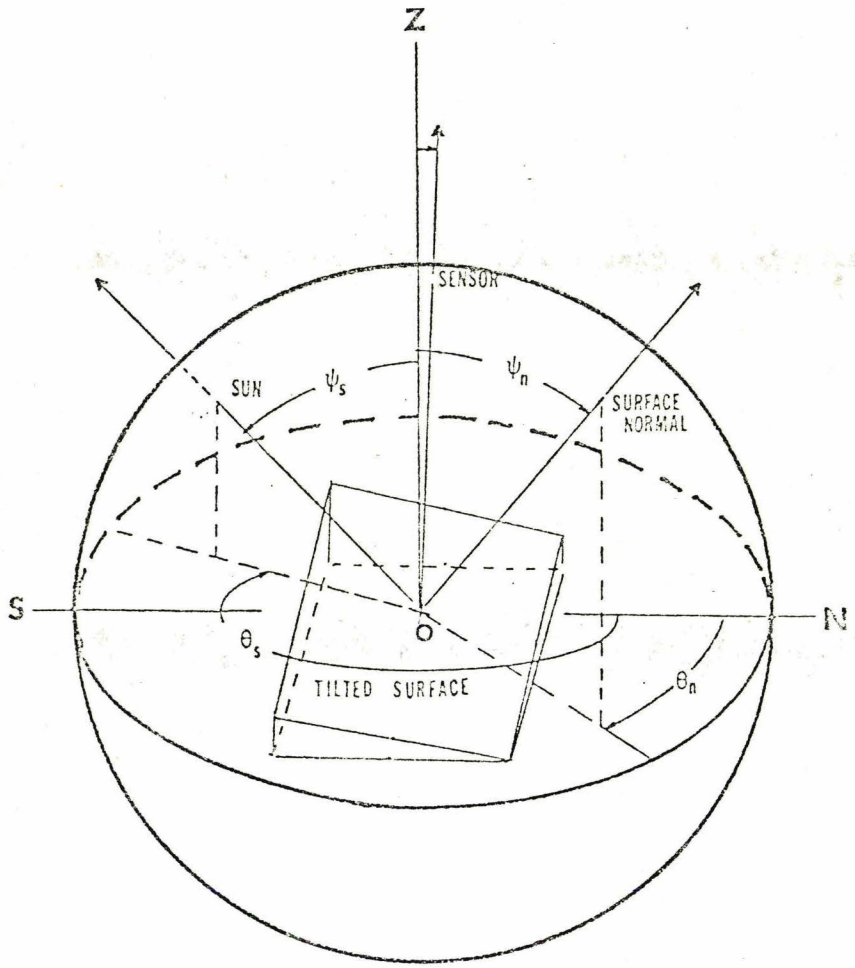

Figure 9. Diagram of geometric relationships between sun and sensor positions.

If:

Ψn = surface normal zenith angle or slope of the terrain surface

Ψs = solar zenith angle

Θn = surface azimuth or aspect angle

and

Θs = solar azimuth angle,

then since the satellite has essentially a vertical view angle, the effective incidence angle, i, and exitance angle, e, from the surface are defined by:

$$\cos i = \cos \Psi s \cos \Psi n + \sin \Psi s \sin \Psi n \cos (\Theta s - \Theta n)$$

and

$$\cos e = \cos \Psi n$$

The phase angle, α, defined as the angle between the sensor and the illumination source, is simply the solar zenith angle in this case and is a constant for the data under consideration.

If the surface behaves as a Lambertian scatterer, the measured satellite response, Bs, is related to the effective normal response, Bn, by:

$$Bs = Bn \cos i \tag{4}$$

However, as we have seen in an earlier section, a more general relationship is given by the Minnaert function:

$$Bs\ (\lambda, \alpha, i, e) = Bn\ (\lambda, \alpha) \cos^{k(\alpha)} i \cos^{k(\alpha)-1} e \tag{5}$$

where

λ = wavelength

k = Minnaert constant for the material type under consideration.

k controls the type of scattering dependence and is related to surface roughness. If k = 1 equation (5) reduces to expression (4), a Lambertian surface. Very large values of k imply strong specular scattering. Values of k unequal to 1.0 imply a combination of diffuse and specular scattering. Expression (5) is evaluated at each wavelength λ. Thus, a strong test of the Lambertian assumption can be made by first linearizing equation (5) and then obtaining the regression value for k. That is:

$$Bs \cos e = Bn \cos^k i \cos^k e$$

$$\log (Bs \cos e) = \log Bn + k \log (\cos i \cos e)$$

letting $y = \log (bs \cos e)$

$x = \log (\cos i \cos e)$

$b = \log (Bn)$

we obtain $y = kx + b$

A t-test of significance can then be made for the slope coefficient, k.

Equations (4) and (5) may also be inverted to develop backward radiance correction transformations for topographic slope and aspect. That is:

Using the Lambertian Assumption:

$$Bn = Bs/\cos i \tag{6}$$

Using the Minnaert relationship:

$$Bn = (Bs \cos e) / (\cos^k i \cos^k e) \tag{7}$$

In this study we first evaluate the Minnaert k coefficient by regression analysis and then apply both correction procedures (6) and (7) to evaluate their likely effect on image classification.

2.4.2 Data Reduction and Analysis

Figure 10 is a reduced orthophotograph of the study site used in this analysis. The study area is located in the Front Range of the Rocky Mountains about 5 miles (8 km) west of Fort Collins, Colorado (Figure 10). The dominant features include sedimentary rock formations uplifted into hogbacks in the east, high steep mountains of metamorphic and igneous rock to the west and Horsetooth Reservoir located in the east-central portion of the study site. Site elevations range from about 4500 ft (1370 m) to 7400 ft (2255 m) with a slope range of 5-50%. In general, gentle, east facing slopes are found in the northeast, and steeper, southwest and northwest facing slopes occur in the west portion of the area.

Vegetative cover in the mountains is primarily ponderosa pine (*Pinus ponderosa*) with understory and open areas consisting of grasses and shrubs. There are also lesser areas of some riparian vegetation. Horsetooth Reservoir occupies approximately 2.5×10^3 acres (1.0×10^3 ha) and lies in a north-south direction across the study site.

An August 15, 1972 Landsat image of the study site was obtained for radiometric analysis. The solar zenith angle at image acquisition was 37 degrees; solar azimuth was 114 degrees. The Landsat image was first geometrically corrected to a scale of 1:24,000 using a nearest-neighbor algorithm. Grey level printouts of each multispectral band were then overlaid on a 1:24,000 quadrangle map of the study site published by the United States Geological Survey in 1962. A 1970 quandrangle centered orthophoto for the study site was also available for comparison. Image to ground registration was improved locally by comparing image gray tones for such distinctive morphological features as stream patterns, rock

Figure 10. Horsetooth, Colorado study site.

Mark Hurd
AERIAL SURVEYS, INC.
[illegible] PENNSYLVANIA AVENUE SOUTH
MINNEAPOLIS, MINNESOTA [illegible]

"THIS PHOTO WAS PREPARED FOR THE COLORADO STATE PLANNING OFFICE AND WAS FINANCED IN PART THROUGH AN URBAN PLANNING GRANT FROM THE DEPARTMENT OF HOUSING AND URBAN DEVELOPMENT, UNDER THE PROVISIONS OF SECTION - 701 OF THE HOUSING ACT."

SCALE 1:24,000

1 1/2 0 1 MILE

1000 0 1000 2000 3000 4000 5000 6000 7000 FEET

DATE OF PHOTOGRAPHY: 1970

State of Colorado

HORSETOOTH RESERVOIR, COLO.
0203

outcroppings, and water bodies to the topographic map. Once registration between the computer grey level printouts and the topographic map was obtained, a grid-cell overlay with cell dimensions approximately equal to the digital Landsat map (1.1 acre) was constructed.

An initial selection of 364 Landsat picture elements (pixels) was made from this overlay representing ponderosa pine samples. These pixels were then examined with regard to their cover homogeneity and a further subsection of 76 pixels made. These 76 pixels were circumscribed by pixels having similar radiance values and were located in the center of areas of relatively similar slope and aspect. This procedure further minimized any extraneous effects of remaining misregistrations between the Landsat observations and the grid cell overlay. The topographic slope, Ψn, and aspect, Θn, were then numerically computed for each of these 76 pixels and merged with their radiance values, Bs, for MSS bands 4, 5, 6 and 7.

Figures 11, a through d, show the scatter of the data in each spectral band as displayed in a Minnaert plot.

2.4.3 Results

A regression equation to the linearized version of the Minnaert function was computed for each wavelength band on the 76 points displayed in Figure 11. The results are shown in Table 7. In all cases the Minnaert constant, k, is significantly less than 1.0 at the 95% confidence level.

We, therefore, conclude that for the range of incidence angles, 30 to 80 degrees, and exitance angles, 0 to 45 degrees, studied, the Lambertian assumption for the Landsat response is invalid.

Figure 11a.

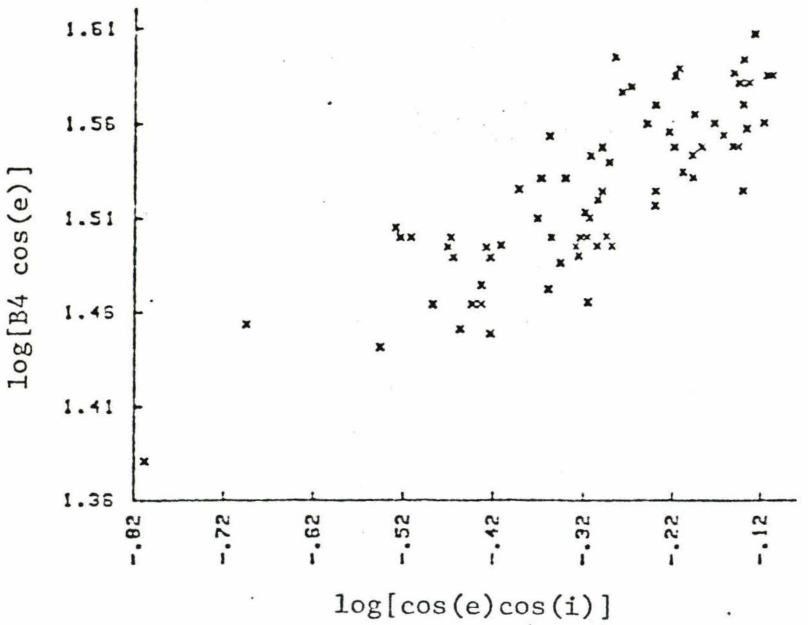

Figure 11b.

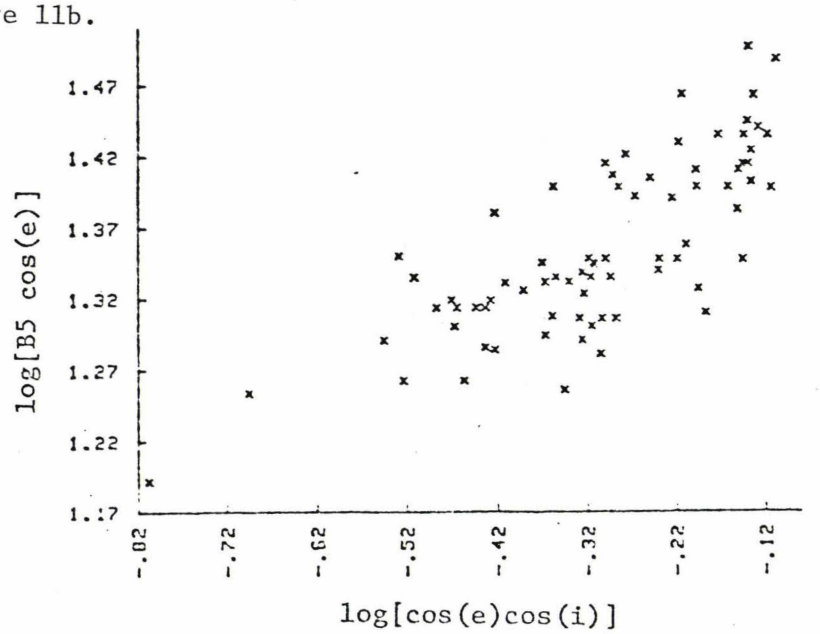

Figure 11. Minnaert plots of Lansat MSS data for ponderosa pine.

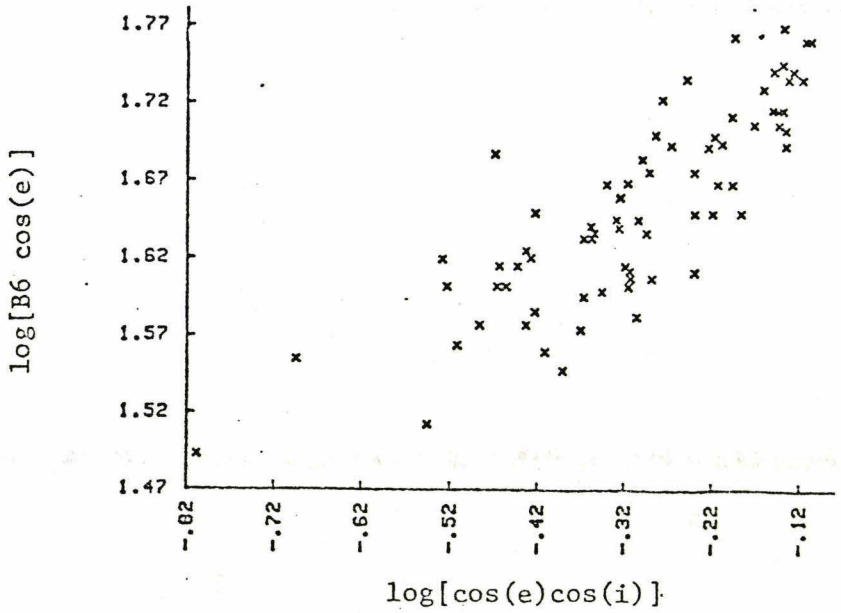

Figure 11c.

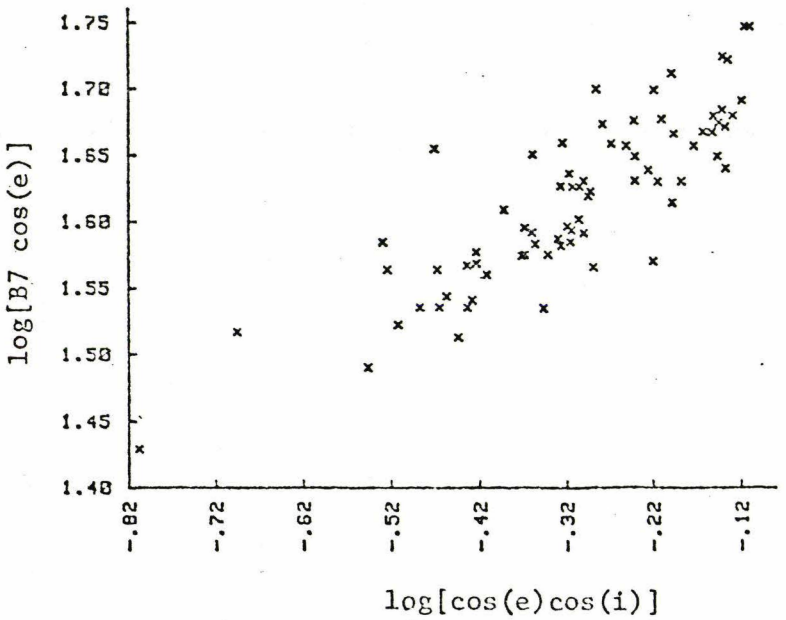

Figure 11d.

For comparison, a regression equation for the 76 pixels utilizing the simple, but incorrect, Lambertian function was also computed. As expected, Table 8 indicates that significantly less of the Landsat variation is explained by this procedure than by employing the Minnaert function.

2.4.4 Discussion and Recommendations

Figure 12 shows the original Landsat responses, (+) as a function of the cosine of the incidence angle for each spectral band versus the Landsat response as corrected by the transformation given by equation (7). It is evident that this correction procedure only slightly modifies the data but does lead to a more level response versus the varying effective solar incidence angle. Consequently, we have appeared to remove this extrinsic source of radiance variation.

In contrast, Figure 13 shows the effect of applying the correction transformation of equation (3) as suggested by Struve. It is evident that, in reality, this procedure introduces more variation into the data. Consequently, it would be better to leave the data uncorrected than apply this transformation which illustrates the inherent dangers involved in applying procedures which may be based on assumed, but incorrect, hypothesis; in this case, the Lambertian assumption.

Figure 14, displays the Minnaert corrected Landsat response versus the original data for each spectral band. It is evident that the Minnaert procedure leads to a nearly linear transformation for our example. Such a near-linear relationship would help explain the success often obtained by the empirical channel ratio methods referenced earlier. If the linear relationships for each spectral band possess similar slopes and if these

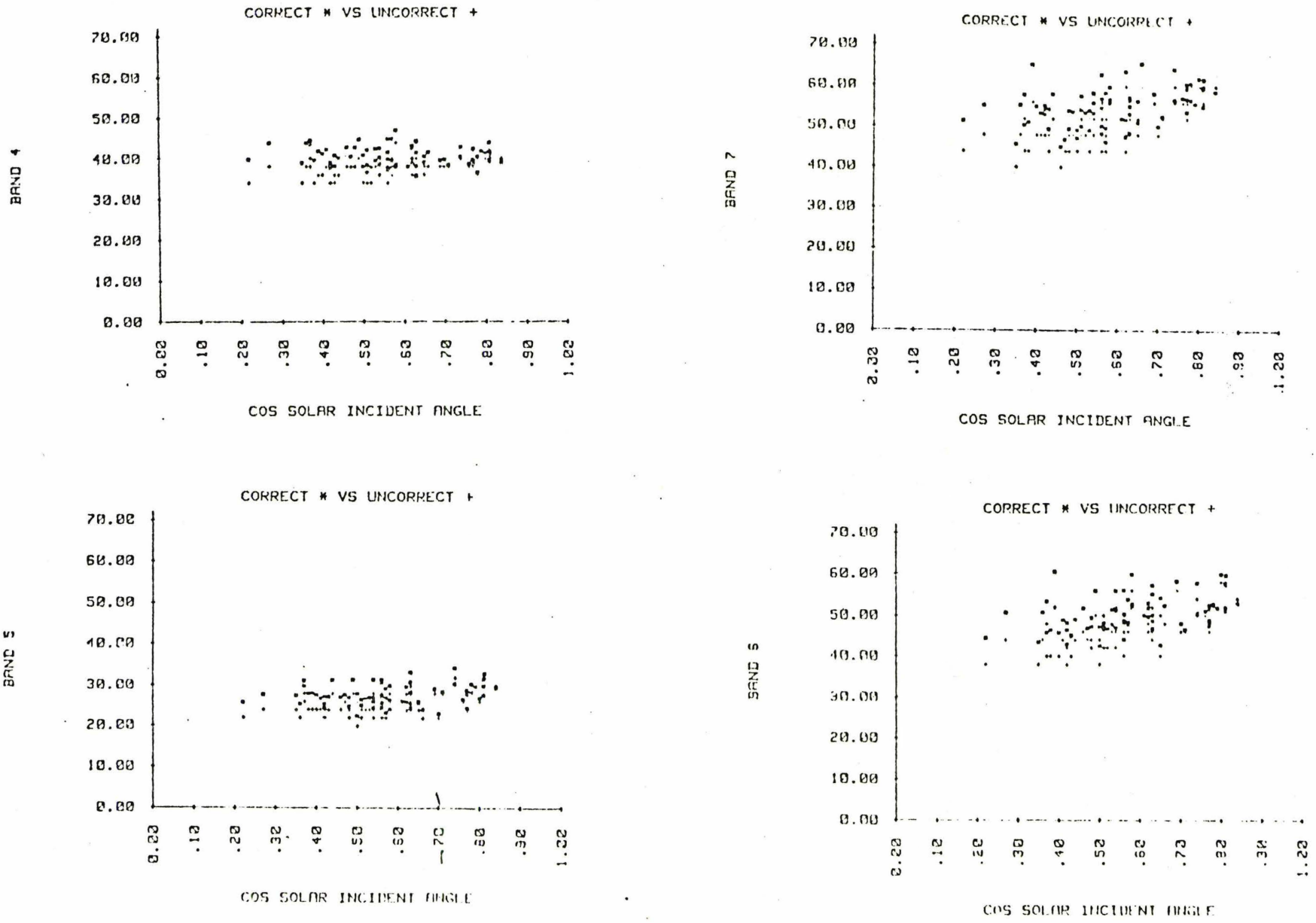

Figure 12. Minnaert corrected and uncorrected Landsat MSS data versus cosine of solar incident angle.

Table 7. Minnaert regression relationships for each Landsat MSS channel.

Landsat Channel	Minnaert Constant, k	t-value (K=1)	R^2
4	0.26	35.2 **	0.68
5	0.33	20.9 **	0.59
6	0.38	22.1 **	0.72
7	0.37	21.7 **	0.68

** Significant at the 95% confidence level with 75 degrees of freedom.

Table 8. Linear R^2 values for regression of Landsat MSS channels versus cos i (Lambertian Assumption) and for the Minnaert relationship.

Landsat Channel	R^2	
	Minnaert	Lambertian (cos i)
1	0.68	0.32
2	0.58	0.35
3	0.71	0.48
4	0.68	0.50

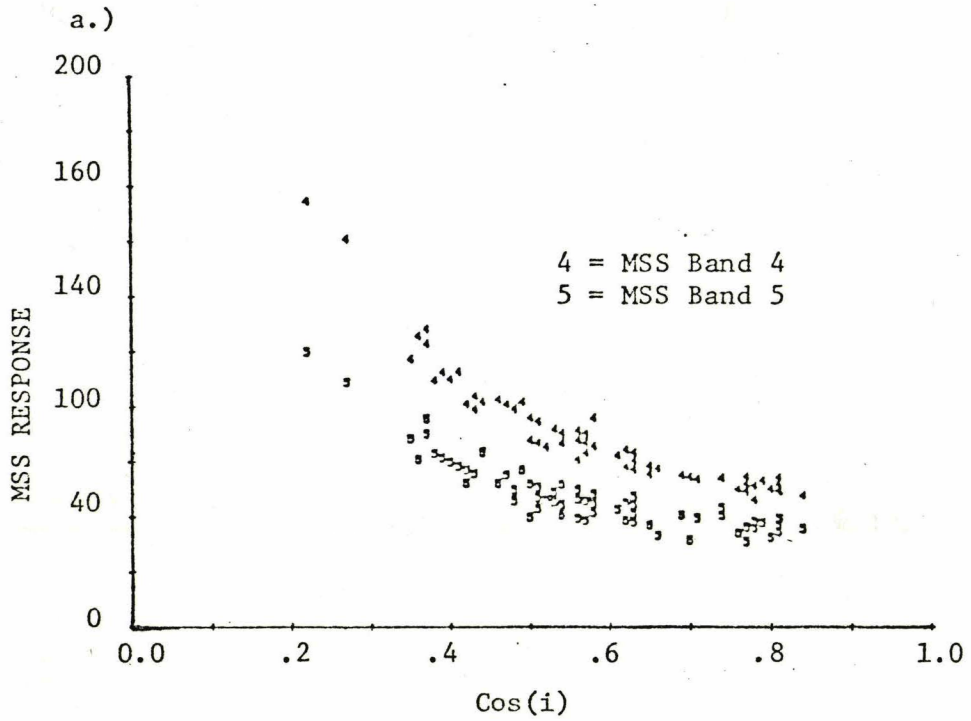

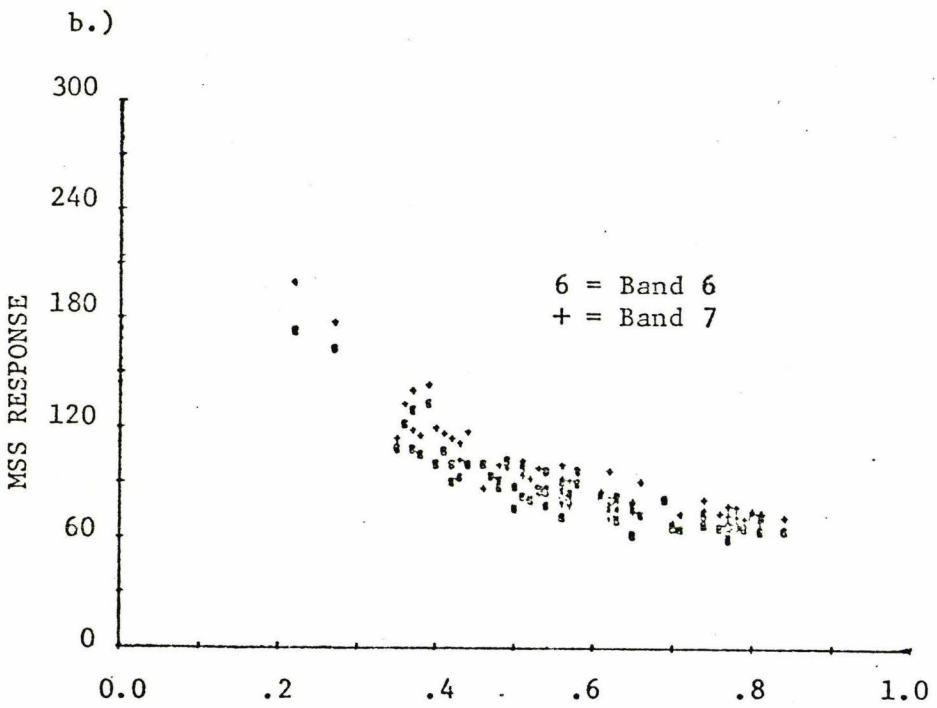

Figure 13. Lambertian corrected Landsat MSS data versus uncorrected Landsat data.

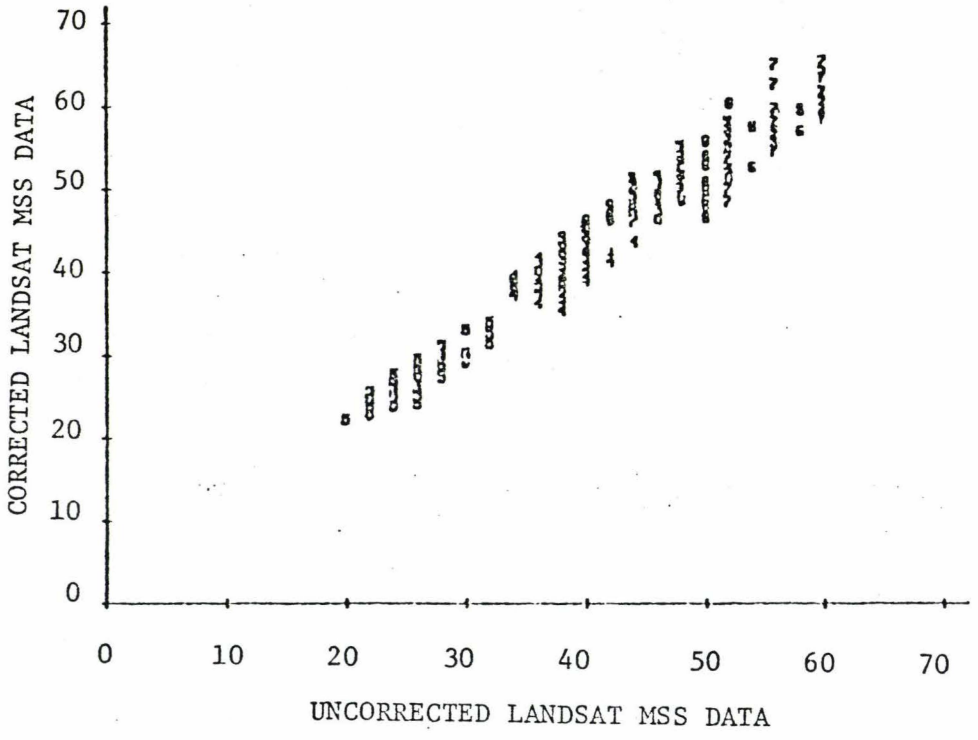

Figure 14. Minnaert corrected Landsat MSS data versus uncorrected Landsat data.

slopes are constant over material type (not just the ponderosa samples shown in Figure 14), channel ratio would remove or enhance much of the topographic variation.

This study has conclusively shown that the Lambertian assumption is not strictly valid for Landsat data. However, many further questions need to be addressed. Specifically:

i) Are there ranges of exitance or incidence angles for which the Lambertian assumption is more nearly valid?

The aircraft analysis of Section 2.3 and modeling results of Section 3.0 indicate that this is the case if the incidence angles are restricted to 40 degrees. Preliminary analysis of the Landsat data also indicate that a much higher Minnaert coefficient is obtained, $k = 0.70$, if such restrictions are made.

ii) How does k vary with material type?

iii) Can an average k coefficient be determined?

iv) What is the actual effect of applying the suggested correction procedures to Landsat classification?

v) Can the correction procedure, if restricted to a single material type, be used to effect enhanced change detection in that class?

3.0 CANOPY MODELING

The solar radiation vegetation canopy model (SRVC) developed by Oliver and Smith (1972) physically accounts for variations in sun angle, sensor view angle, optical properties and geometry of canopy components. The model was originally developed for grassland canopies, but has been modified to handle woody vegetation canopies. Further modifications were necessary in order to examine the model as a potential tool for determining stratification criteria in forested areas where variations in topography occur. In addition, the Minnaert function (Minnaert, 1941) was applied to model simulated responses as a quantitative test for Lambertian behavior.

3.1 Model Modification

Two modifications were made to the original SRVC model. The first made it possible for a woody vegetation canopy to be treated, while the second allowed the background surface to be tilted.

The model now handles vegetation canopies which consist of two components; branches and needles. In the modification, the leaf (needle) angle distributions and the branch angle distributions within each canopy layer are weighted by their relative proportion of the total surface area within the layers and summed. This yields a total component angle distribution which is used by the model to calculate the probability of an interaction of a source radiation vector with a component of any type.

If a source vector encounters a canopy element, further calculations are necessary in order to determine whether a leaf (needle) or branch was hit. In this case, the probability of gap for either branches, PGB,

or leaves, PGL, are separately calculated for the particular source vector. The normalized probability of hit for leaves, PHL, and branches, PHB, are then given by:

$$PHL = \frac{(1.0 - PGL)}{(1. - PGB) + (1. - PGL)}$$

and

$$PHB = \frac{(1.0 - PGB)}{(1. - PGB) + (1. - PGL)}$$

If a random number, between 0 and 1, is selected and is less than PHL, an interaction with a leaf (needle) is assumed; otherwise a branch element was encountered. The appropriate component angle distribution and optical scattering properties are then used to calculate the overall scattered flux.

In order to apply the SRVC model as a tool for determining stratification criteria where topographic variations exist, modifications to the treatment of the background were necessary. The original model treated only the case where the underlying surface was horizontal. The modified version allows a slope and aspect to be input, computes the direction cosines to the normal of that surface, and finally treats the sloping background in a manner similar to that in which inclined leaves are treated as they are "hit" by incoming radiation. The major difference between the treatment of a leaf and the slope is that no radiation is allowed to strike the "back side" of the slope.

The modification to the treatment of the background follows the following logic:

In general, for any angle, Θ_r bin, the power reflected is given by:

$$P(\Theta_r{}^1) = \int_0^{2\pi} \int_{\Theta^1_r - \Delta\Theta_r}^{\Theta_n{}^1 + \Delta\Theta_r} \frac{\rho E}{\pi} (\hat{a} \cdot \hat{r}) \sin \Theta_r \, d\Theta_r \, d\phi_r$$

Where: $\hat{a}$ represents the direction cosines of the slope, $\hat{r}$ represents the direction cosines of the source, E is irradiance and ρ is surface reflectance.

Since $(\hat{a} \cdot \hat{r})$ equals $\cos i$, by testing for $\cos i < 0$ the cases where the back side of the slope is hit are determined and subsequently ignored. Flux calculations for the allowable cases when $\cos i > 0$ utilize the equation given above. In the original model, when $\hat{a}$ was constant for a horizontal surface, the $(\hat{a} \cdot \hat{r})$ factor could be represented by $\cos \theta_r$, and the power equation reduced to:

$$P(\theta_r^1) = \rho E \left[\sin^2(\theta_r^1 + \Delta\theta_r) - \sin^2(\theta_r^1 - \Delta\theta_r)\right]$$

3.2 Model Simulations

A series of model analyses were performed to provide initial validation of the model for a specified range of conditions, to examine background topographic effects, and to summarize view angle effects using Minnaert analysis. Field data from both the Leadville, Colorado and the Colorado State Forest Service were utilized in the analysis.

3.2.1 Benchmark Comparisons

Two initial test simulations for forest canopy reflectance prediction were made using the solar radiation vegetation canopy model for July 1, 1977 (1116 hours). For these simulations, data from Leadville, Colorado at the M-3 site were input to the model. The vertical reflectance in six wavelength bands were obtained for a group of four lodgepole pine trees. Branch and needle angle distribitions, branch and needle area indices, understory reflectance, needle reflectance and transmission, branch reflectance and transmission, direct/diffuse

irradiance ratio, global irradiance, latitude, solar declination, and time of day were input to the modified model. The data are presented in Appendix A. All of the above data were obtained from the M-3 site except for needle transmission and reflectance. These were obtained from a one sample reflectance and transmission curve of a ponderosa pine needle. The above data were also condensed to one component and a run made. In the latter simulation, only the needle reflectance and transmission curves were used along with a combined needle-branch angle distribution. Simulation results for both runs for six discrete wavelengths are shown in Figure 15.

In addition to the above runs three data modules were created for lodgepole pine, Russian Olive, and grass. A brief description of the data and results for each module required to run the SRVC model follows:

1. Lodgepole Pine

A three layered, one canopy component simulation was made for the vertical reflectance in six wavelength bands for the group of four lodgepole pine trees at the M-3 site at Leadville, Colorado.

The input data for this run differed from the previous runs as follows. Both branch and needle angle distributions were used. Total component area index for the canopy was 3.2 as contrasted with 5.0 for the above runs. In addition, the lodgepole pine needle reflectance was measured using a Isco Model SR Spectral Radiometer, a mosiac of lodgepole pine needles, and a Barium Sulfate reference panel.

The simulated and measured results for July 1, 1977 (1116 standard time) are presented in Figure 16. It is hypothesized that the method utilized in measuring the needle reflectance which employs a mosaic of needles overestimates the spectral reflectance especially in the near

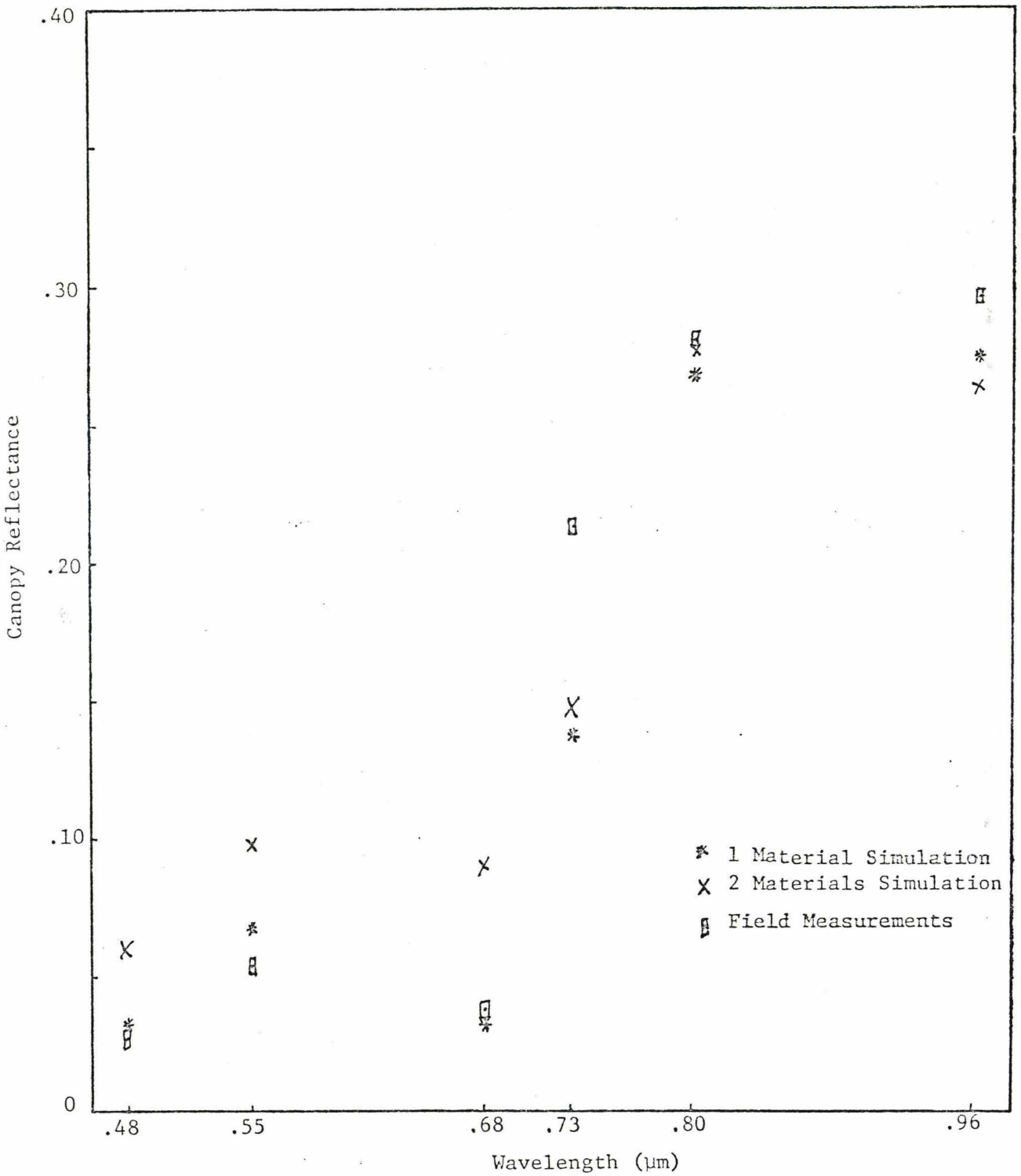

Figure 15. Simulated and measured reflectance of a lodgepole pine canopy for July 1, 1977 (1116 standard time). A one layered simulation was made for both one component, and two components in the canopy.

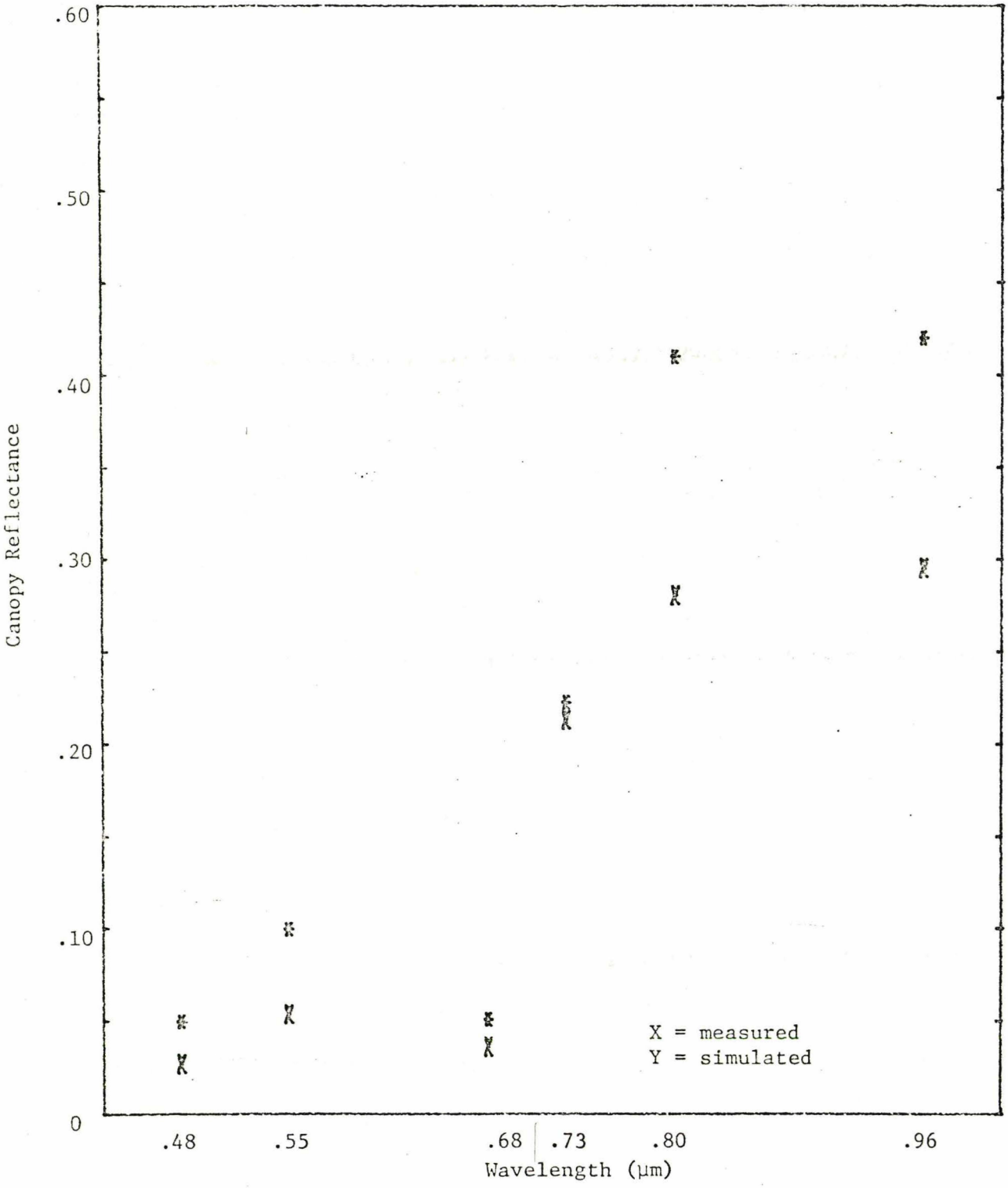

Figure 16. Simulated and measured reflectance of a lodgepole pine canopy for July 1, 1977 (1116 standard time). A three layered, one component simulation was made.

IR region. The measured reflectances for the 0.80 and 0.96 μm bands were 0.77 and 0.80, respectively. More recent measurements indicate that the maximum needle reflectance in the near IR region is approximately 0.68. Thus, the above may explain the relatively large deviations in the near IR between the simulated and measured canopy reflectances in Figure 16.

2. Russian Olive

A one layer, one canopy component simulation was made for the vertical reflectance in six wavelength bands for a single Russian Olive tree at the Colorado State Forest Service Nursery at Fort Collins, Colorado on August 9, 1978 (1030 standard time). Leaf area index, leaf angle distribution, ground reflectance, and leaf reflectance and transmission were measured. The results of the simulated and measured canopy reflectance are presented in Figure 17.

3. Grass

A one layer, one canopy component simulation was made for the vertical reflectance in six wavelength bands for the grass canopy (*Agropyron sp.*) at the Colorado State Forest Service Nursery at Fort Collins, Colorado on May 18, 1978 (0930 standatd time). Leaf area index was estimated visually. A spherical leaf angle distribution was utilized as presented by deWitt (1965) and measured by Smith, Oliver and Berry (1977) on Blue Gamma. Ground reflectance, and leaf reflectance and transmission were measured in the field. The results are presented in Figure 18.

In general, the model yields predictions which follow the trends of the measured data. Near infrared reflectance appears to be

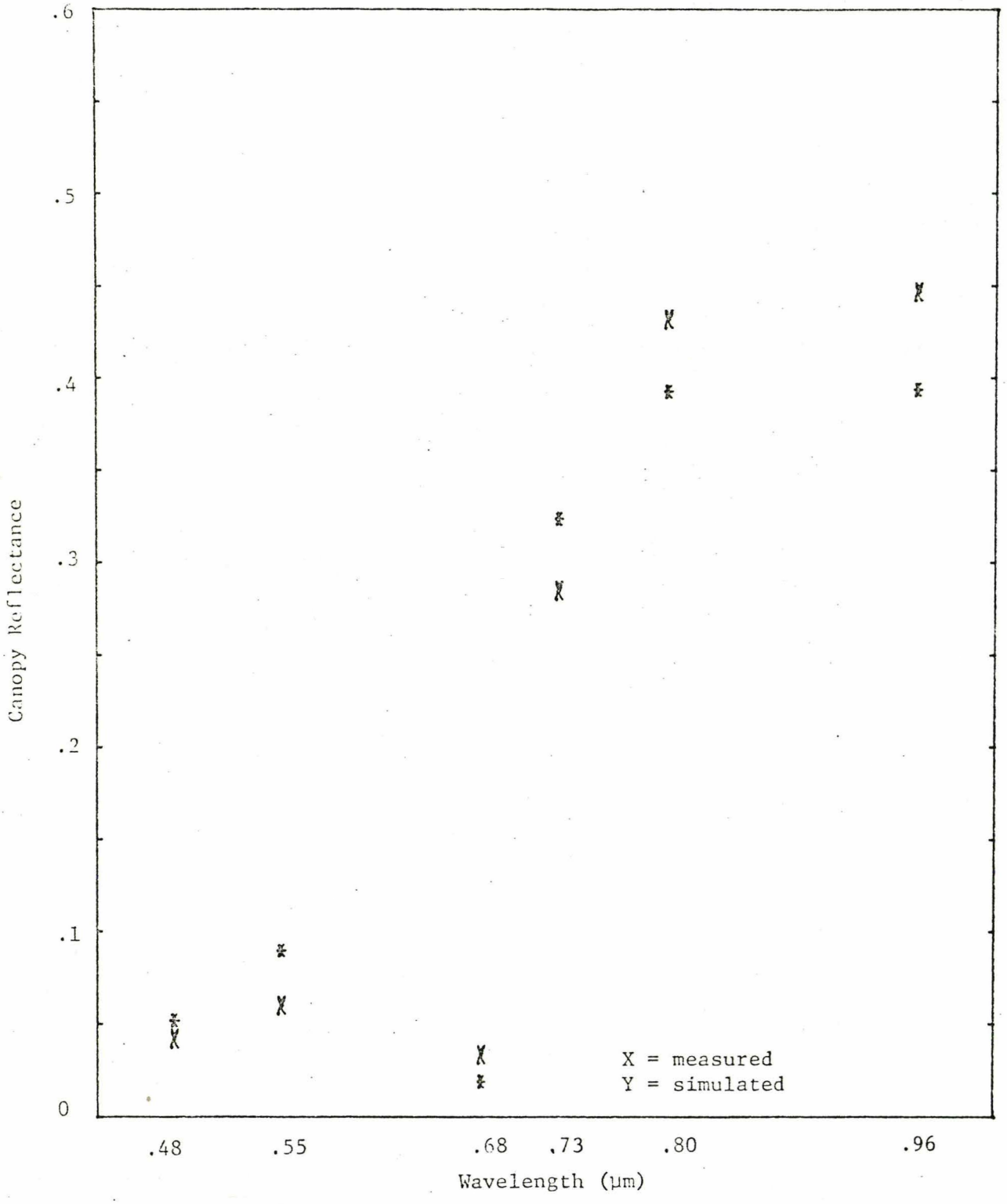

Figure 17. Simulated and measured reflectance of a Russian olive tree for August 9, 1978 (1030 standard time). A one layered, one component simulation was made.

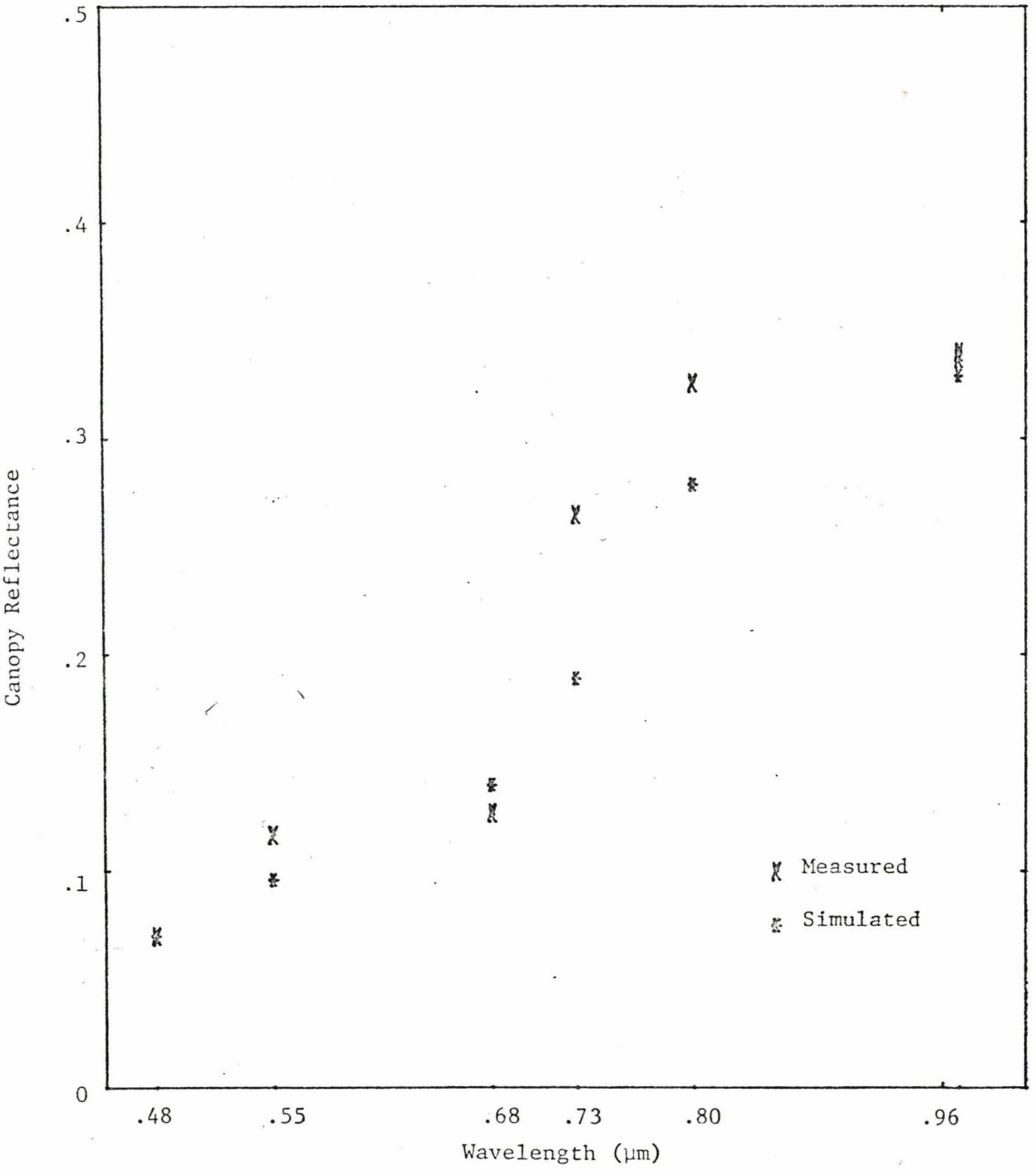

Figure 18. Simulated and measured reflectance of a grass canopy (*Agropyron sp.*) for May 18, 1978 (0930 standard time). A one layered one component simulation was made.

overestimated, particularly for the lodgepole pine canopies. However, this may be a result of inadequate constituent optical measurements.

3.2.2 Background Slope Simulations

Six background slope simulations were made for both Russian olive and Lodgepole pine canopies to test for significant effects on canopy reflectance. The specific slopes analyzed were 5, 15, 25, 35 and 45 degrees. In each case two wavelengths were simulated; The chlorophyll absorption, 0.68 μm, and the near infrared, 0.80 μm. The input data for Russian olive is given in Section D of Appendix A. Mountain Daylight Time was 9:30 a.m.

The response of each canopy at each wavelength was normalized to the flat surface case. The results are given in Figure 19 and 20. These plots indicate no significant effect on canopy reflectance resulting from a tilted background.

These results may be due to two factors. First, the leaf area index for both canopies is high (3.2). Secondly, the model modifications do not incorporate any density variations in the canopy as a function of topographic slope.

3.2.3 Minnaert Analysis

One layer, one canopy component simulations were made for reflectances at nine sensor view angles in two wavelength bands for Russian olive and lodgepole pine canopies at 0930 MDT. Minnaert plots were constructed and are shown in Figures 21 and 22. It should be noted that the phase angle is not a constant. However, for Lambertian or near-Lambertian surfaces, the plots should be independent of phase angle. Figures 23 and 24 show the normalized responses of lodgepole and Russian olive versus the cosine of the exitance angle e. If the response were

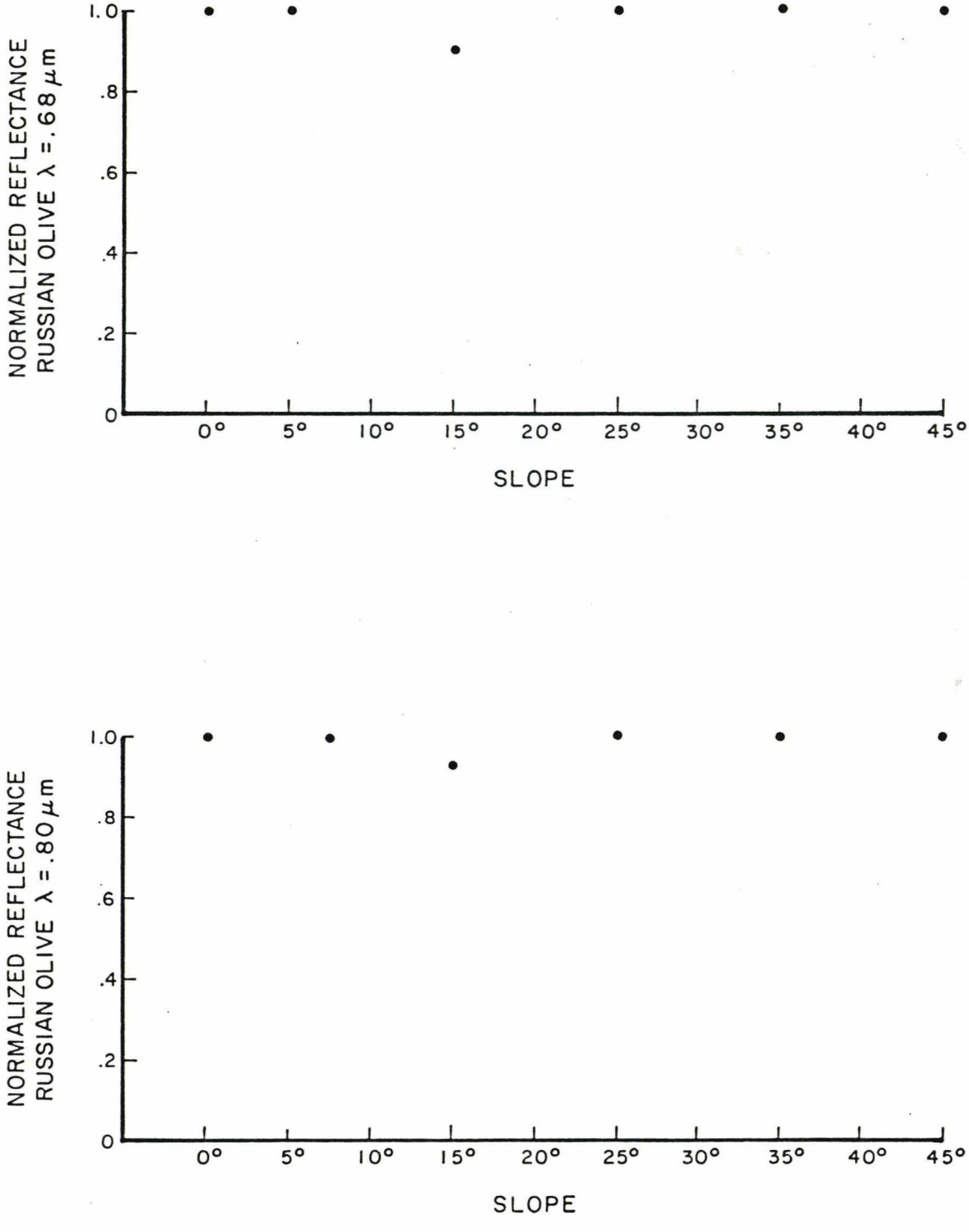

Figure 19. Normalized reflectance versus slope for Russian olive at two wavelengths (.68 and .80μm). Reflectances were normalized to the flat surface case.

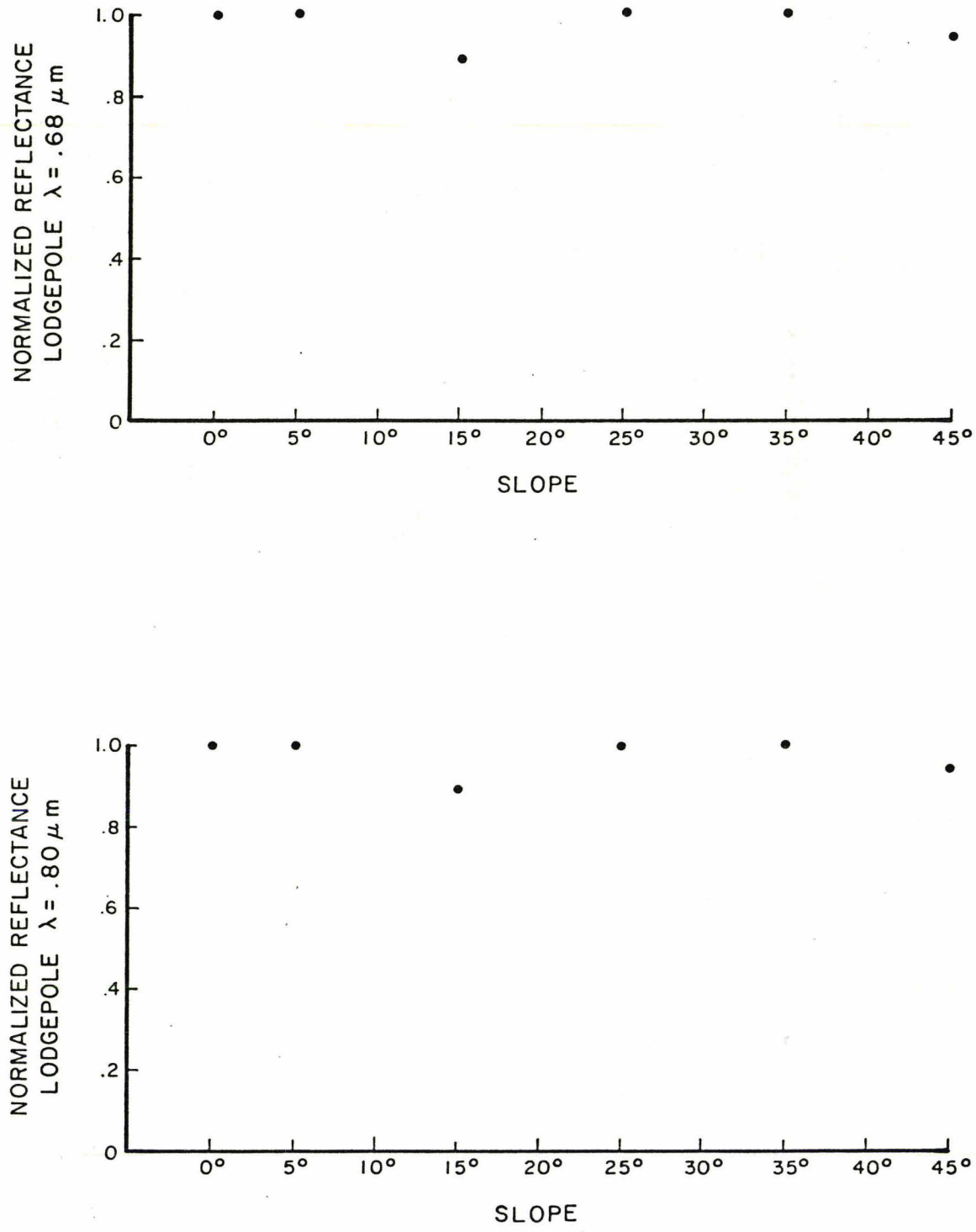

Figure 20. Normalized reflectance versus slope for lodgepole pine at two wavelengths (.68 and .80 μm). Reflectances were normalized against the flat surface case.

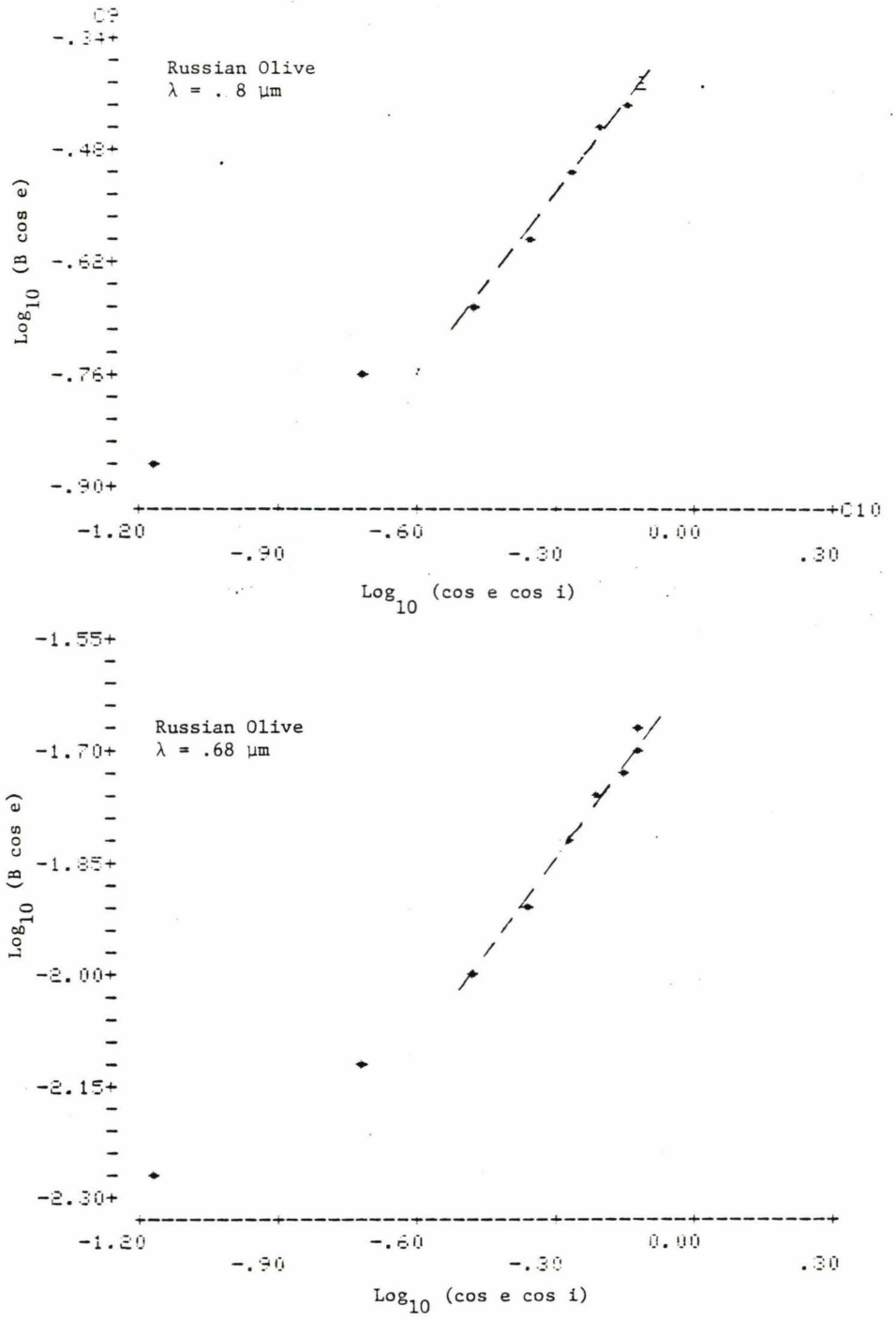

Figure 21. Minnaert plots of simulated Russian olive response in two wavelengths (.68 and .80 μm).

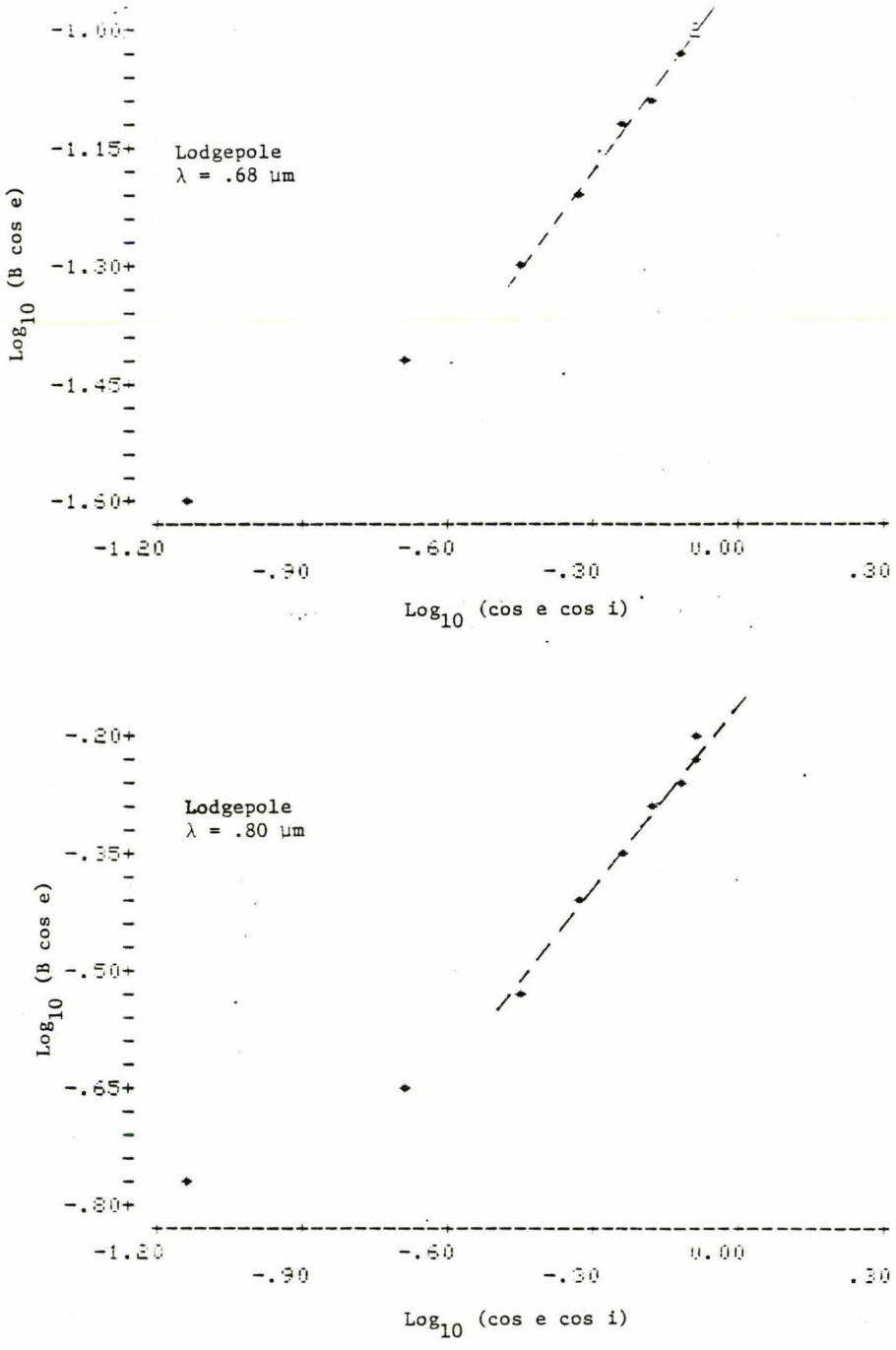

Figure 22. Minnaert plots of simulated lodgepole pine response in two wavelengths (.68 and .80 μm).

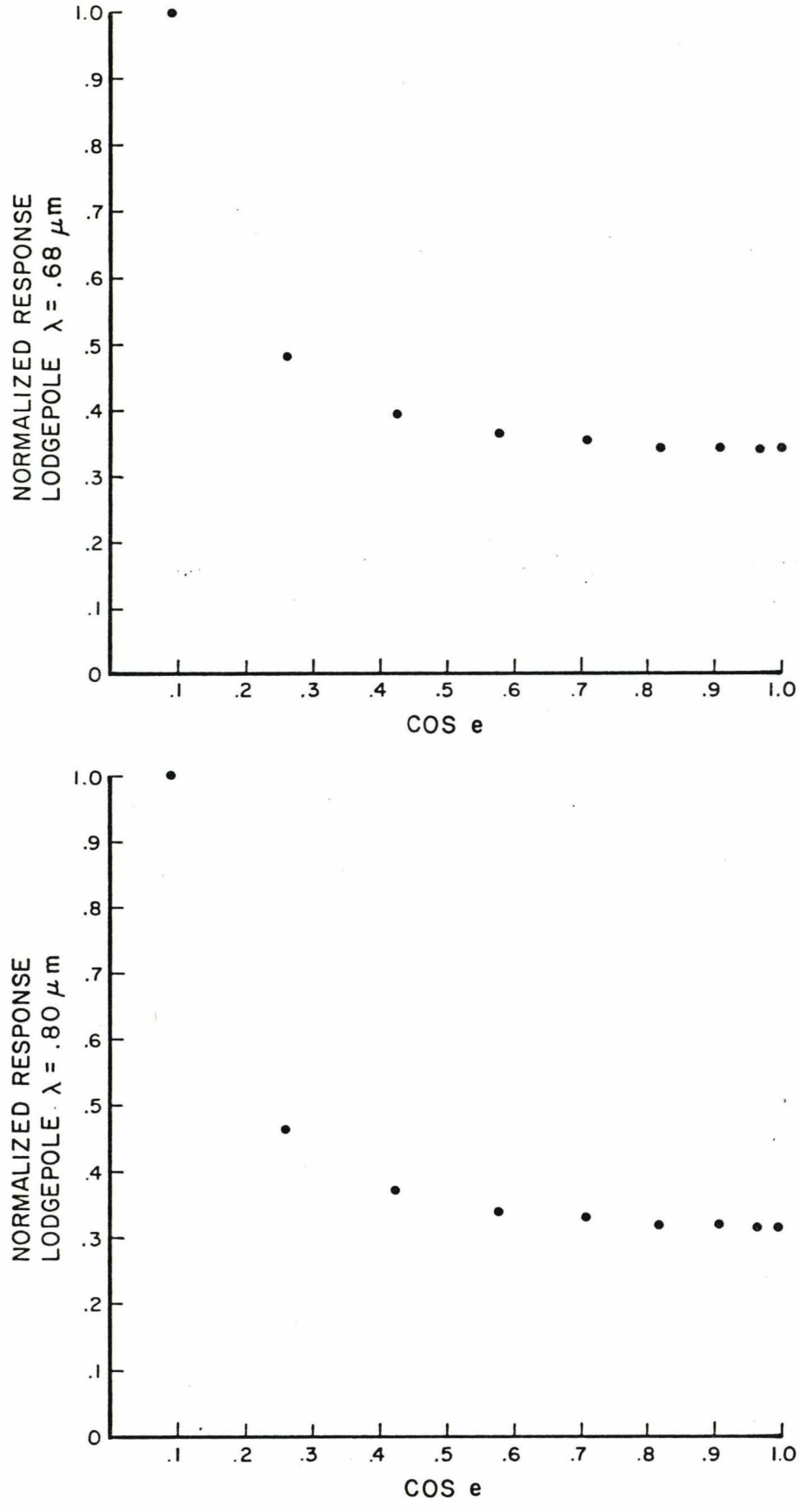

Figure 23. Normalized response versus cos e for lodgepole pine simulated at wavelengths of .68 and .80 μm.

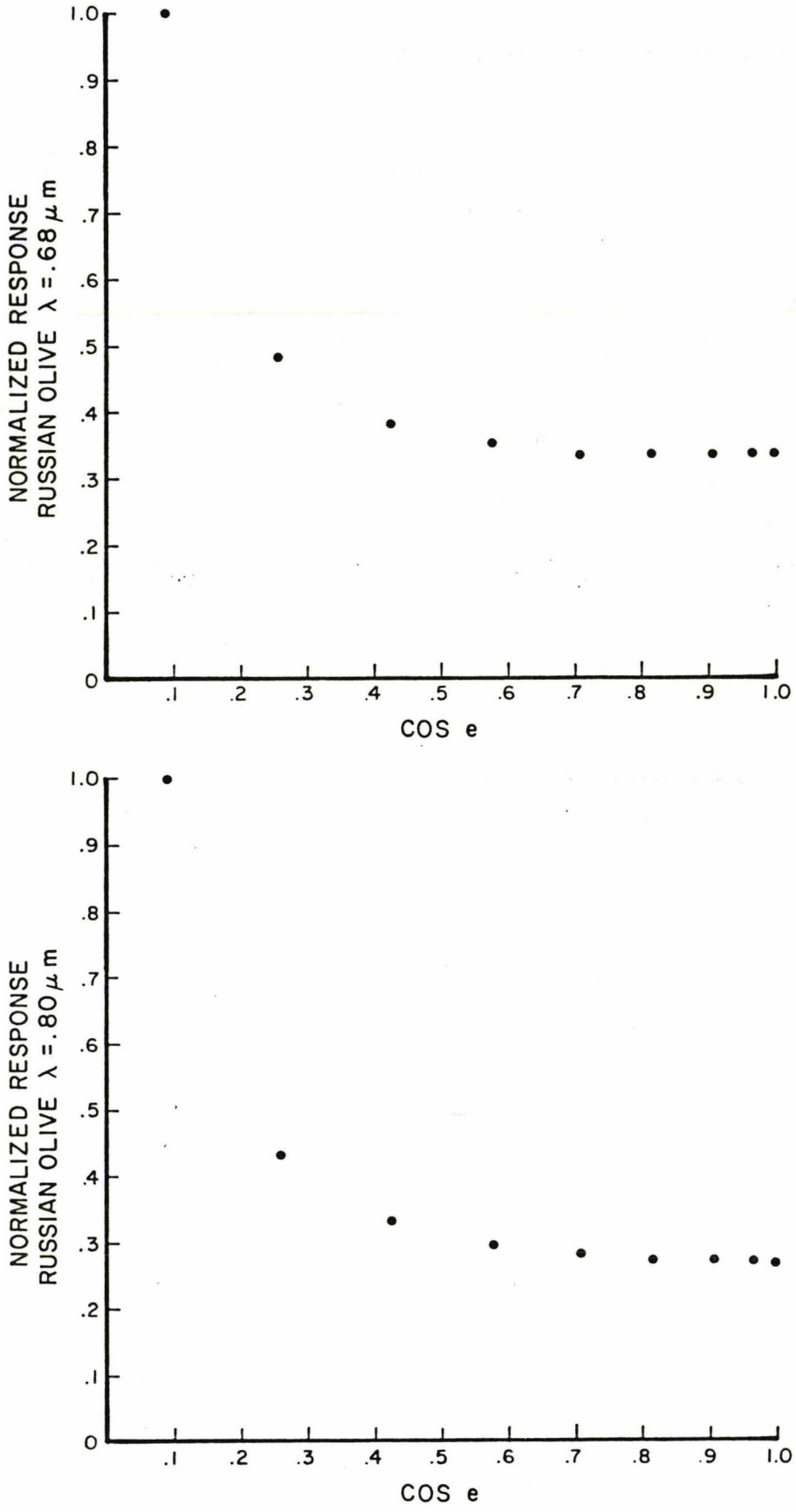

Figure 24. Normalized response versus cos e for Russian olive simulated at wavelengths of .68 and .80 μm.

entirely Lambertian, all points would fall on a horizontal line. As seen the most marked departures occur at steep sensor view angles of 75 to 85 degrees, and less so at 65 degrees, while the rest approximate a Lambertian response. Regression equations developed for these points on the Minnaert plots and the subsequent t-tests presented in Table 9 show that the value of k does not equal one in any of the cases, but does reach .85 for sensor zenith view angles of less than 65 degrees.

3.2.4 Summary

The SRVC model yields predictions which follow the general trends of the measured data. Near infared reflectance appears to be over-estimated, particularly for lodgepole pine canopies, though this may be due to inadequate constituent optical measurements.

The results obtained for simulation of canopies with a background slope indicated that no recommendations for stratification of scenes by topographic variation can be made. It should be noted that the test runs represent special cases in which canopy density remained a constant while in nature, variations in density can be expected.

The Minnaert analysis resulted in rejection of the hypothesis that $k = 1$ for simulated response data. Thus, non-Lambertian behavior is conducted in all cases, though a value of $k = .85$ suggests that it may be near-Lambertian for zenith view angles up to 60 degrees.

Table 9. T-table for two cases of lodgepole pine and Russian olive at two wavelengths.

Case 1. Seven degrees of freedom: sensor view angles from 0 to 85 degrees.

	λ in μm	k Coefficient	Standard Deviation	$t_{K=1}$
Lodgepole	.68	.58	.055	9.1
	.80	.55	.055	9.2
Russian olive	.68	.57	.055	8.9
	.80	.48	.055	10.7

Case 2. Five degrees of freedom: sensor view angles from 0 to 65 degrees.

	λ in μm	k Coefficient	Standard Deviation	$t_{K=1}$
Lodgepole	.68	.83	.02	10.2
	.80	.83	.02	9.2
Russian olive	.68	.85	.03	4.9
	.80	.76	.02	10.1

4.0 CONCLUSIONS AND RECOMMENDATIONS

This study included the analysis of a variety of scene radiance measurements covering different effective terrain geometries and sensor resolutions. Specifically, the following data sets were evaluated:

i) Ground-based Scene Measurements at fixed view angle at nadir, but varying zenith sun angle, 20 to 80 degrees. Sensor resolution was 20 ft (6.1 m) in diameter. Targets included lodgepole pine (*Pinus contorta*), two grass communities, and snow.

ii) Aircraft-based Measurements at varying effective zenith view angles, 0 to 22 degrees, and zenith sun angles, 12 to 40 degrees. Sensor resolution was 12 acres (4.9 ha). Material type was lodgepole pine.

iii) Satellite-based Measurements at varying effective zenith view angles, 0 to 45 degrees, and varying effective zenith sun angles, 0 to 75 degrees. Sensor resolution was 1.1 acre (.45 ha). The target was pondersoa pine (*Pinus ponderosa*).

In addition, an idealized unit area of canopy was simulated under a fixed solar zenith angle and varying zenith view angles, 0 to 85 degrees, using a process-oriented radiative transfer model. Material types modeled were lodgepole pine, Russian olive and grass.

Data sets (i) and (ii) were subject to fluctuations arising from atmospheric and illumination changes. These effects were minimized with the rapid data acquisition rate of Landsat for the study area and are totally absent from the model results. Data sets (ii) and (iii) were obtained from areas of significant topographic relief.

In all cases our analyses verified or rejected the Lambertian assumption for radiance scattering from the terrain materials. In some cases where non-Lambertian behavior was evident we attempted to describe limits in which the assumption is nearly true. For those cases where the phase angle between the sensor and illumination source (actually the dominant solar source) was constant, cases (ii) and (iii), we found it convenient to employ the Minnaert relationship. This relationship yields a more general functional dependence of directional radiance on effective view and source angles. An inverse correction procedure, given a known material type, was suggested from the analysis of satellite data.

Our specific conclusions are:

- For effective zenith or source angles greater than 60 degrees, all materials exhibit strong non-Lambertian behavior. This is particularly true in the chlorophyll absorption band and less in the near infrared.
- For effective angles less than 40 degrees, near Lambertian behavior is approximated.
- For constrained environmental conditions, that is "stable" atmospheric, illumination, and phase angle, the directional radiance properties may be quantified by the Minnaert relationship.
- For snow, phase angle appears to vary linearily with sensor response from 35 to 60 degrees. Estimated slope coefficients show good agreement with values published in the literature.

- The canopy reflectance model follows the general trends of field measurements for lodgepole pine, Russian olive, and grass, but overestimates infrared response.
- In order to adequately model topographic influences on spectral response, canopy density variations must be included.

These conclusions lead us to the following recommendations:

- Initially, further analysis should be restricted to aerial (multi-band) photography.

  We recommend this data medium because it more nearly incorporates constant phase angle, possesses a wide range of film sensitivities and spatial resolutions, facilitates the incorporation of ancillary spatial information, and is of great practical utility.

  We specifically recommend the evaluation of the Minnaert approach for specific material types as a normalization procedure in mountainous terrain. Such a procedure, if effective would provide enhanced imagery to recognize more subtle changes occuring in terrain type.
- In the long run, it is also appropriate to examine potential correction procedure employing directional dependence as given by the Minnaert function to satellite imagery. Satellite imagery offers a good medium that satisfies the constant phase angle requirement, but offers pragmatic difficulties in the necessary data handling in order to fully evaluate the Minnaert approach.

REFERENCES

Aldrich, R. C., R. W. Dana, and E. H. Roberts. 1977. Inventory of forest resources (including water) by multilevel sampling. Type III Final Report (March 1975-July 1977). Goddard Space Flight Center, Greenbelt, MD, 20771).

Berry, J. K., F. J. Heimes, and J. A. Smith. 1978. A portable instrument for simultaneous recording of scene composition and spectral reflectance. Opt. Eng. 17(2):143-146.

Binder, A., and J. Jones. 1972. Spectrophotometric studies of the photometric function, composition and distribution of the surface materials of Mars. J. of Geophys. Res., Vol. 77, No. 17, pp. 3005-3020.

Crane, R. B. 1971. Preprocessing techniques to reduce atmospheric and sensor variability in multispectral scanner data. Proc. of the 7th Int. Symp. on Remote Sensing of Environment, V. II, pp. 1345-1355.

Duggin, M. J. 1977. Likely effects of solar elevation on the quantification changes in vegetation with maturity using sequential Landsat imagery. Applied Optics 16:521-523.

Gillespie, A. R., and A. B. Kahle. 1977. Construction and interpretation of a digital thermal inertia image. Photo. Eng. Rem. Sens. XLIII (8):938-999.

Hapke, B., and H. Van Horn. 1963. Photometric studies of complex surfaces, with applications to the moon. J. Geo. Res. 68(15):4545-4570.

Hart, T. 1978. Reduction of topographic shadow effects in Landsat by division of mean brightness. M.S. Thesis, Earth Resources Dept., Colorado State University, Fort Collins, Colorado.

Heimes, F. J. 1977. Effects of scene proportions on spectral reflectance in lodgepole pine. M.S. Thesis, Earth Resources Dept., Colorado State University, Fort Collins, Colorado.

Heimes, F. J., and J. A. Smith. 1977. Spectral variability in mountain terrain. Final Report, USDA Rocky Mountain Forest and Range Exp. Sta., Cooperative Agreement 16-625-CA, 115 pp.

Hoffer, R. 1974. Natural resources mapping in mountainous terrain by computer analysis of ERTS-1 satellite data. LARS/Purdue University, West Lafayette, IN.

Kreibel, K. T. 1978. Measured spectral bidirectional reflection properties of four vegetated surfaces. Applied Optics 17(2):253-258.

Minnaert, M. 1941. The reciprocity principle in lunar photometry. Astrophys. J. 93:403-410.

Monteith, J. L., and G. Szeicz. 1961. The radiation balance of bare soil and vegetation. Quart. J. R. Met. Soc. 87:159-170.

Proctor, J. T. A., W. J. Kyle, and J. A. Davies. 1972. The radiation balance of an apple tree. Can. J. Bot. 50(8):1731-1740.

Ryan, T. A., B. L. Joiner, and B. F. Ryan. 1976. MINITAB student handbook. Wadsworth, Inc., Belmont, CA 341 pp.

Smith, J. A., and R. E. Oliver. 1972. Plant canopy models for simulating composite scene spectroradiance in the .4 to 1.04 μm region. Proc. Eight Inter. Symp. on Remote Sensing of Envir., U. of Mich., Ann Arbor, pp. 261- 274.

Smith, J. A., and R. E. Oliver. 1974. Effects of changing canopy directional reflectance on feature selection. Applied Optics 13(7):1599-1604.

Stewart, J. B. 1971. The albedo of a pine forest. Quart. J. R. Met. Soc. 97:561-564.

Struve, H., W. Graham, and H. West. 1977. Acquisition of terrain information using Landsat multispectral data. Report 1 of series, Technical report M-77-2, Mobility and Environ. System Laboratory U.S. Army Engineering Waterway Experiment Station, Vicksburg, MS 39180, 50 pp.

Veverka, J. 1972. Effects of surface roughness on the photometric properties of Mars. ICARUS 16:281-288.

Veverka, J. 1973. The photometric properties of natural snow and snow covered plants. ICARUS 20:304-310.

Veverka, J., J. Gougen, S. Yang, and J. L. Elliot. 1978. How to compare the surface of Io to laboratory samples. ICARUS 34:63-67

Vincent, R. K. 1973. Spectral ratio imaging methods for geological remote sensing from aircraft and satellites. Proc. of Symp. on Management and Utilization of Remotely Sensed Data, American Society of Photogrammetry, Sioux Falls, SD, October, pp. 377-397.

Young, A. T., and S. A. Collins. 1971. Photometric properties of the mariner cameras and of selected regions on Mars. J. Geophys. Res. 76(2):432-437.

Appendix A

Data Required For SRVC Simulations

A. Initial lodgepole pine run for 1 layer and 1 component.

B. Initial lodgepole pine run for 1 layer and 2 components.

C. Lodgepole pine run for 3 layers and 1 component.

D. Russian olive run for 1 layer and 1 component

E. Grass run for 1 layer and 1 component

A) Initial lodgepole pine run for 1 layer and 1 component

1) LAI = 5.06

2) Needle angle distribution

Inclination angle	Probability
0	0.000
5	.001
10	.003
15	.007
20	.012
25	.017
30	.022
35	.029
40	.036
45	.044
50	.054
55	.065
60	.076
65	.085
70	.092
75	.099
80	.102
85	.153
90	.103

3) Ground reflectance

Band (μm)

.48	.55	.68	.73	.80	.96

Reflectance

.093	.151	.176	.348	.450	.478

4) Needle reflectance

Band (μm)

.48	.55	.68	.73	.80	.96

Reflectance

.091	.192	.090	.378	.732	.753

5) Needle transmission

Band (μm)

.48	.55	.68	.73	.80	.96

Transmission

.002	.011	.003	.035	.064	.053

B) Initial lodgepole pine run for 1 layer and 2 components

1) LAI = 4.51

2) BAI = 0.55

3) Needle angle distribution

Inclination angle	Probability
0	0.000
5	.001
10	.003
15	.007
20	.012
25	.017
30	.022
35	.029
40	.036
45	.044
50	.054
55	.065
60	.076
65	.085
70	.092
75	.099
80	.102
85	.153
90	.103

4) Branch angle distribution

Inclination angle	Probability
0	0.000
5	.065
10	.127
15	.126
20	.113
25	.099
30	.086
35	.072
40	.062
45	.051
50	.038
55	.033
60	.028
65	.024
70	.020
75	.017
80	.018
85	.019
90	.000

5) Ground reflectance

Band (μm)

.48	.55	.68	.77	.80	.96

Reflectance

.093	.151	.176	.348	.450	.478

6) Needle reflectance

Band (μm)

.48	.55	.68	.77	.80	.96

Reflectance

.091	.192	.090	.378	.732	.753

7) Needle transmission

Band (μm)

.48	.55	.68	.77	.80	.96

Transmission

.002	.011	.003	.035	.064	.053

8) Branch reflectance

Band (μm)

.48	.55	.68	.77	.80	.96

Reflectance

.125	.189	.219	.235	.423	.375

C) Lodgepole pine run for 3 layers and 1 component

Layer 1

1) LAI = .90

2) Component angle distribution

Inclination angle	Probability
0	.086
5	.088
10	.089

Inclination angle	Probability
15	.089
20	.081
25	.082
30	.081
35	.073
40	.061
45	.061
50	.051
55	.049
60	.039
65	.030
70	.021
75	.021
80	.011
85	.001
90	.000

Layer 2

1) LAI = 1.70

2) Component angle distribution

Inclination angle	Probability
0	.082
5	.094
10	.083
15	.082
20	.081
25	.080
30	.079
35	.069
40	.067
45	.057
50	.048
55	.048
60	.039
65	.039
70	.030
75	.020
80	.011
85	.001
90	.000

Layer 3

1) LAI = .60

2) Component angle distribution

Inclination angle	Probability
0	.119
5	.112
10	.098
15	.093
20	.080
25	.068
30	.066
35	.056
40	.055
45	.046
50	.046
55	.036
60	.036
65	.027
70	.027
75	.018
80	.010
85	.000
90	.000

All layers

1) Ground reflectance

Band (μm)

.48	.55	.68	.73	.80	.96

Reflectance

.093	.151	.176	.348	.450	.478

2) Needle reflectance

Band (μm)

.48	.55	.68	.73	.80	.96

Reflectance

.072	.244	.130	.645	.774	.804

3) Needle transmission

Band (μm)

.48	.55	.68	.73	.80	.96

Transmission

.002	.011	.003	.035	.064	.053

D) Russian olive run for 1 layer and 1 component

1) LAI = 3.2

2) Leaf angle distribution

Inclination angle	Probability
0	.09
5	.09
10	.08
15	.08
20	.08
25	.08
30	.08
35	.07
40	.07
45	.06
50	.05
55	.05
60	.04
65	.03
70	.03
75	.02
80	.01
85	.00
90	.00

3) Ground reflectance

Band (μm)

.48	.55	.68	.73	.80	.96

Reflectance

.074	.108	.127	.256	.329	.364

4) Leaf reflectance (top)

Band (μm)

.48	.55	.68	.73	.80	.96

Reflectance

.072	.126	.027	.430	.527	.542

5) Leaf transmission

Band (μm)

.48	.55	.68	.73	.80	.96

Transmission

.000	.004	.000	.023	.145	.054

E) Grass canopy run for 1 layer and 1 component

1) LAI = 1.2

2) Leaf angle distribution

Inclination angle	Probability
0	.004
5	.007
10	.014
15	.022
20	.029
25	.035
30	.042
35	.048
40	.054
45	.059
50	.064
55	.069
60	.072
65	.076
70	.078
75	.080
80	.082
85	.083
90	.083

3) Ground reflectance

Band (μm)

.48	.55	.68	.73	.80	.96

Reflectance

.097	.122	.198	.220	.318	.368

4) Leaf reflectance

Band (μm)

.48	.55	.68	.73	.80	.96

Reflectance

.080	.234	.095	.500	.638	.659

5) Leaf transmission

Band (μm)

.48	.55	.68	.73	.80	.96

Transmission

.003	.014	.045	.023	.048	.053